R. & M. No. 3310

MINISTRY OF AVIATION

AERONAUTICAL RESEARCH COUNCIL
REPORTS AND MEMORANDA

Further Experimental Investigations of the Characteristics of Cambered Gothic Wings at Mach Numbers from 0·4 to 2·0

By L. C. Squire, Ph.D.

LONDON: HER MAJESTY'S STATIONERY OFFICE
1963
FIFTEEN SHILLINGS NET

Further Experimental Investigations of the Characteristics of Cambered Gothic Wings at Mach Numbers from 0·4 to 2·0

By L. C. SQUIRE, Ph.D.

COMMUNICATED BY THE DEPUTY CONTROLLER AIRCRAFT (RESEARCH AND DEVELOPMENT), MINISTRY OF AVIATION

*Reports and Memoranda No. 3310**
December, 1961

Summary.

The wind-tunnel tests on cambered gothic wings reported in Reports and Memoranda No. 3211 have been extended to include the effects of changes in design lift coefficient and of changes in spanwise camber without changes in camber incidence distribution.

It was found that the camber was successful in that the flow was attached over the whole wing at the design lift. Also at the design lift the lift-dependent drag was close to the predicted values. However, the lift-dependent drag of the uncambered wing was also close to this value so that the benefit of camber on lift/drag ratio was very small. At subsonic speeds the cambered wings were less stable than the uncambered wing; also the changes of stability with incidence and Mach number were greater, particularly near $M = 1 \cdot 0$.

Changes in spanwise camber, without changes in incidence distribution, do not alter the force characteristics near the design lift, but do alter the off-design characteristics.

1. *Introduction.*

In connection with the design of slender wings for high lift over drag, an experimental investigation of slender-wing models with curved leading edges and various types of camber is being made in the 3 ft Tunnel at the Royal Aircraft Establishment, Bedford. The results of tests at supersonic speeds on the first two wings in this programme were presented in Ref. 1. Both of these wings were of gothic planform, aspect ratio 0·75, with the same thickness distribution. One wing was uncambered and the other was cambered by Weber's method[2] to have completely attached flow and low drag-due-to-lift at the design lift coefficient $\{(C_L)_d = 0 \cdot 1\}$. Tests, both at supersonic speeds[1] and at low speeds[3], on this first cambered wing showed that the large droop of the wing near the leading edge retarded the development of leading-edge separation at off-design conditions.

In the present report tests at supersonic speeds on two more cambered gothic wings are described. On both these wings the amount of leading-edge droop was decreased by reducing the design lift coefficient to 0·05; the two designs were obtained by integrating the camber incidence distribution with two different initial conditions (*see* Section 2.1 for details).

The report also includes results of tests on all four wings at subsonic and transonic speeds.

* Previously issued as R.A.E. Tech. Note No. Aero. 2803—A.R.C. 23,724.

2. *Details of Tests.*

2.1. *Description of Models.*

All the cambered wings tested in the present programme were designed by a method described by Weber[2]. One feature of this design method is of particular relevance in the present programme. The camber design is based on 'slender, thin wing' theory which yields, for a given load distribution, a formula for the local incidence distribution, $\partial/\partial x\{z(x, y)\}$. This incidence distribution must then be integrated with respect to x to obtain the camber surface. The integration introduces an arbitrary function of y (the spanwise co-ordinate); this function Weber fixed by making the wing trailing edge straight, i.e., by putting z = constant at $x = c_0$. For structural and aerodynamic reasons it may be desirable to modify this condition, and the fourth wing in the present series is designed to find the effect of a change in this function of y (*see* Fig. 4 and below).

Full details of the four wings are given in Table 1 and in Figs. 1 to 4, where the wings are designated by the numbers 1 to 4. Wing 1 is the uncambered wing and wing 2 the cambered wing of Ref. 1. Wing 3 has the same type of camber incidence distribution as wing 2, but the amount of camber (and hence of leading-edge droop) has been decreased by reducing the design C_L to 0·05. Wing 4 has the same camber incidence distribution as wing 3, but differs in actual shape as the camber surface was obtained by making the wing straight (i.e., z = constant) at $x = 0{\cdot}8c_0$ instead of at $x = c_0$ as on wing 3.

Wing 1 was made of steel throughout, but the three cambered wings were made of glasscloth and Araldite formed onto a metal core. In all models a small circular body of 1·35 inches diameter was used at the rear of the model to shield the balance and sting support (Fig. 1).

2.2. *Range of Tests.*

The tests were made in the transonic and supersonic test sections of the 3 ft Tunnel at R.A.E., Bedford. The range of force tests, consisting of measurements of lift, drag and pitching moment, is given in the following table:

Wings	Test Section	Mach numbers	Incidence Range (1° steps)
3	Supersonic	1·42, 1·61, 1·82, 2·0	−5° to +12°
4	Supersonic	1·42, 1·61, 1·82, 2·0	−5° to +10°
1 and 2	Transonic	0·4, 0·7, 0·8, 0·85, 0·9, 0·94, 0·98, 1·02, 1·25, 1·30	−5° to +10°
3	Transonic	0·4, 0·7, 0·9, 0·94, 0·98, 1·02, 1·25, 1·30	−2° to +13°
4	Transonic	0·4, 0·7, 0·9, 0·94, 0·98	−2° to +10°
3 and 4	Nominal supersonic test section with unshaped (flat) wall	0·4	−2° to +17°

All tests were made at a Reynolds number of 2×10^6 based on aerodynamic mean chord.

The force tests on wings 1 and 2 at supersonic speeds[1] with free transition showed that extensive regions of laminar flow occurred on the wings at low incidence. It was also found that turbulent flow over the whole wing could be obtained with bands of carborundum along the leading edge; these bands of carborundum did not change the lift or pitching moment, but did increase the drag. For all the present force tests therefore, transition was fixed with bands of carborundum along the full length of the leading edge; the bands were approximately 0·5 in. wide normal to the leading edge and started 0·125 in. inboard of the edge. Two grades of carborundum were used, the grain size being 0·007 in. for $M = 1{\cdot}42$ and above, and 0·003 in. for lower speeds. Oil-flow tests suggested that these bands had in fact fixed transition throughout the incidence range at all Mach numbers.

During initial tests on wings 1 and 2 in the transonic test section, large fluctuating stresses occurred in the balance*. Near $M = 0{\cdot}80$ these reached a peak value which was considered dangerous; hence no measurements were made on wings 3 and 4 between $M = 0{\cdot}70$ and 0·90.

In addition to force tests, oil-flow investigations were made at various Mach numbers and incidences; details are given in the following sections. Early tests with and without roughness bands showed no significant changes in vortex position or shape. Thus, since the main region of interest in the flow development occurs near the leading edge, the main oil-flow tests were made without roughness bands.

2.3. *Reduction and Accuracy of Results.*

Force results have been reduced to the usual coefficient form; on all four wings the reference areas and chords are based on the common planform. Pitching-moment coefficients are given about the quarter-chord point of the mean aerodynamic chord. The drag has been corrected to a base pressure on the minimum body equal to free-stream static pressure.

No corrections have been applied for wind-tunnel interference or for angularity of the tunnel flow. The former correction is zero at Mach numbers above $M = 1{\cdot}3$ since the reflection of the bow wave strikes the model support well downstream of the model base. Below this Mach number the interference effects are probably small, except near $M = 1{\cdot}0$, where the measured speed may have been somewhat in error. Also, at $M = 1{\cdot}25$ and 1·30 measurements of base pressure suggested that flow at the model base was still affected by wall interference. Hence the drag results at these Mach numbers were considered not reliable and have not been presented.

Apart from tunnel interference it is estimated that the accuracy of the results is as follows:

$C_L \pm 0{\cdot}003$

$C_m \pm 0{\cdot}0005$

$C_D \pm 0{\cdot}0004$ at $C_L = 0$
$\pm 0{\cdot}001$ at $C_L = 0{\cdot}3$ } $M \geqslant 1{\cdot}42$

$\alpha \pm 0{\cdot}05°$ from measurement, together with a possible error of $\mp 0{\cdot}1°$ from flow angularity.

The errors in drag measurement may be slightly greater at subsonic speeds owing to the balance vibration mentioned in last section; also all the results at $M = 0{\cdot}4$ are subject to larger errors than those listed above owing to the low level of loading at this Mach number.

* The vibrations which were responsible for these fluctuating stresses occurred when the natural frequency of the model system (i.e., model, balance and sting) corresponded with a frequency of main disturbances in the tunnel air stream: they had no other aerodynamic significance.

3. *Presentation and Discussion of Results.*

Full results for wings 1 and 2 at supersonic speeds are given in Ref. 1. Force results for wings 3 and 4 at supersonic speeds and for all four wings at subsonic and transonic speeds are given in the present report. Graphical presentation has been adopted (*see* Figs. 5 to 8 and 12 to 20).

In discussing the results some cross-reference to the earlier report is obviously necessary. In order to keep this reference to a minimum the discussion has been divided into four parts. In the first part, results for wing 3 at supersonic speeds are discussed, and the behaviour of this wing is compared with that already described for wings 1 and 2 in Ref. 1. The other three sections then deal with topics which are less related to the subject matter of Ref. 1.

3.1. *Flow and Force Development on Wings* 1 *and* 3 *at Supersonic Speeds.*

The variations of C_L with α, and of C_m, C_D and L/D with C_L for wings 1 and 3 are compared in Figs. 5 to 8. Oil-flow photographs for wing 3 at a series of incidences at $M = 1{\cdot}61$ and $M = 2{\cdot}0$ are given in Figs. 9a, 9b and 10. Comparable photographs for wing 1 (though not at identical incidences) are shown in Figs. 11a and 11b.

Before discussing the results it should be recalled that in the investigation[1] of the flow development on wing 2 at supersonic speeds it was found that the flow remained attached at the leading edge, and over the whole wing, for an incidence range on both sides of the design incidence; also the lift-curve slopes were linear throughout the test range. At the same Mach numbers the flow separated from the leading edge of wing 1 at very low incidence and the separated sheet rolled into a vortex which produced a non-linear lift contribution; the size of this contribution decreased with increase of Mach number.

The results plotted in Figs. 5 to 8 show that apart from a displacement of the curves the force results for wing 3 are similar to those of wing 1, and again the non-linearity of the lift and moment curves decreases with increase in Mach number.

The oil-flow photographs (Figs. 9a and 9b) at $M = 1{\cdot}61$ for wing 3 show that separations do occur on this wing at small incidences away from the design point ($C_L = 0{\cdot}05$), but there is still a small incidence range in which the flow is attached, for example at $\alpha = 3{\cdot}1°$ ($C_L = 0{\cdot}070$) and $\alpha = 2{\cdot}0°$ ($C_L = 0{\cdot}045$) the flow was attached on both surfaces of the wing*. (The actual flow patterns at $\alpha = 2°$ are almost identical to those at $\alpha = 3{\cdot}1°$ and so are not presented.) Above these incidences the lower-surface oil pattern remains similar to that at $\alpha = 3{\cdot}1°$ but a separation occurs on the upper surface. The vortex associated with this separation is quite small but can be seen in the photograph for $\alpha = 4{\cdot}2°$ ($C_L = 0{\cdot}097$) over the outer half of the leading edge where the attachment and secondary separation lines are clearly visible[4]. At higher incidences ($\alpha = 6{\cdot}3°$ and $8{\cdot}4°$) separation starts nearer the apex and the attachment and secondary separation lines move inboard. It should be noted that at $\alpha = 6{\cdot}3°$, i.e., approximately 4° above the design point, the shape and position of

* In the interpretation of these photographs it should be noted that the regions of unmoved oil which exist at most incidences represent regions of attached laminar flow. For example on the lower surface at $\alpha = 3{\cdot}1°$ the oil has formed streamlines near the leading edge due to the high shear in the laminar attached flow there. Farther inboard the oil is unmoved except for two regions at the rear of the wing where the well defined oil lines indicate that transition has occurred. It should be noted that roughness which was used to fix transition in the force tests was removed for the visualisation tests in order to obtain details of the flow in the immediate vicinity of the edge. Thus the transition changes do not occur in the force tests.

the vortex is similar to that on the plane wing at $\alpha = 4°$ (Fig. 11b). At incidences below $\alpha = 2°$ separation occurs along most of the leading edge, and a vortex lies along the lower surface (*see* photograph for $\alpha = 0$).

At $M = 2{\cdot}0$ the photographs (Fig. 10) of oil flow do not show a single large vortex, even at $\alpha = 8°$; instead at this incidence the oil flow could be interpreted as showing a series of small vortices running back over the wing. However, the lift-curve slope for this Mach number begins to increase at incidences above about 6° incidence, the rate of increase being less than at lower Mach numbers. Thus it would appear that although a single vortex has not formed at 8° incidence, a change in the flow has nevertheless taken place which causes an increase in lift-curve slope.

On wing 1 there appears to be little change in the surface flow pattern as the Mach number is increased from $1{\cdot}6$ to $2{\cdot}0$; the only change being that the vortex starts nearer the wing apex at the lower Mach number. Thus the decrease in non-linear lift on this wing with increase in Mach number is probably associated with changes in the vortex strength, which might not produce large changes in the surface flow pattern, rather than with the disappearance of the vortex as on wing 3.

3.2. *Effects of Camber-Design Lift Coefficient.*

3.2.1. *Lift and pitching moment.*—The variation of C_L with α and of C_m with C_L for wings 1 and 3 is compared in Figs. 5 and 6 for Mach numbers between $M = 1{\cdot}42$ and $M = 2{\cdot}0$. Similar curves for wings 1, 2 and 3 between $M = 0{\cdot}4$ and $M = 1{\cdot}3$ are given in Figs. 12 and 13, 15 and 16, and 18 and 19.

These figures show that in addition to giving a positive no-lift angle and a non-zero pitching moment at zero lift, camber also causes a displacement to higher lift coefficient of the minimum slope of the lift and moment curves. This minimum slope occurs at, or near, the condition of flow attachment and the non-linear behaviour of the curves away from this condition is associated with the growth of leading-edge separations. In order to study this non-linearity in more detail results at Mach numbers of $0{\cdot}7$, $0{\cdot}9$, $1{\cdot}02$, $1{\cdot}61$ and $2{\cdot}0$ have been replotted in the form of $(C_L - \bar{C}_L)$ against $(\alpha - \bar{\alpha})$, and $(C_m - \bar{C}_m)$ against $(C_L - \bar{C}_L)$ {Figs. 21 and 22}, where $\bar{\alpha}$, $\bar{C}_L$ and $\bar{C}_m$ are values of α, C_L and C_m corresponding to the minimum lift-curve slope.

Fig. 21 shows that the lift development about $\bar{\alpha}$ is similar for all three wings although there are some small differences between the wings. For example, at supersonic speeds the lift-curve slope of wing 2 at $\alpha = \bar{\alpha}$ is larger than that of the other wings, also the lift of wing 2 is linear throughout the test range, and at the highest values of $(\alpha - \bar{\alpha})$ wing 3 has the greatest lift. Fig. 21 also includes linear lift-curve slopes as given by slender-wing theory ($C_L = \pi/2\ A\alpha$) and, at supersonic speeds, by not-so-slender-wing theory[5,6]. Also included are curves of $C_L = \pi/2\ A\alpha + 4\alpha^2$; $4\alpha^2$ being the non-linear lift increment derived by Smith[7]. At $M = 0{\cdot}7$, $C_L = \pi/2\ A\alpha + 4\alpha^2$ slightly overestimates the total lift of wing 1 whereas at $M = 1{\cdot}02$ it provides a slight underestimate. However, at $M = 1{\cdot}02$ the initial lift-curve slope is higher than $\pi/2A$ so that $4\alpha^2$ is still a fair approximation to the non-linear lift increment. At $M = 1{\cdot}6$ the lift is again in fair agreement with Smith's estimate; however, a study of the curves shows that this agreement is fortuitous since the initial lift-curve slope is much greater than $\pi/2\ A$, and is in fact in excellent agreement with the not-so-slender value.

The curves of $C_m - \bar{C}_m$ against $C_L - \bar{C}_L$ show an almost complete collapse at supersonic speeds (Fig. 22), but at subsonic and transonic speeds the range of C_L about $\bar{C}_L$ in which the aerodynamic centre remains at a constant position before moving back, increases with camber-design lift

coefficient. This difference in behaviour is presumably associated with the changes in leading-edge separation discussed in Section 3.1. The effect of this increase in range of constant aerodynamic-centre position is clearly illustrated in Figs. 23 and 24, where the variations of centre-of-pressure position with C_L at fixed Mach number, and of centre-of-pressure position with Mach number for fixed C_L are compared for the three wings*. It should be noted, however, that the large forward shift in centre-of-pressure position which occurs on both cambered wings near $M = 1{\cdot}0$ is associated both with a forward shift of aerodynamic centre (*see* Fig. 22) and with a decrease in $\bar{C}_m$ in this speed range. Reasons for the forward shift in aerodynamic centre near $M = 1{\cdot}0$ have not been found. The fact that the effect only occurs on the cambered wings rules out wind-tunnel interference as the main cause, although the actual magnitude of the forward shift may be influenced by tunnel-constraint effects.

3.2.2. *Drag.*—Drag polars for wings 1, 2 and 3 at transonic and subsonic speeds are presented in Figs. 14, 17 and 20. Similar curves for wings 1 and 3 at supersonic speeds are shown in Fig. 7. All results are for wings with fixed transition. Comparative drags are plotted for fixed Mach number in Fig. 25 and for fixed C_L in Fig. 26.

From Fig. 25 it can be seen that at negative and low positive lift coefficient, the drag of wing 1 is less than that of the cambered wings, but that with increase in C_L the drag of wing 1 becomes greater than that of the cambered wings. The drag of wing 3 $\{(C_L)_d = 0{\cdot}05\}$ is always less than that of wing 2 $\{(C_L)_d = 0{\cdot}10\}$. The large increase in zero-lift drag of wing 2 as compared with wings 1 and 3 is mainly due to the extensive flow separations which occur on the lower surface of wing 2 at lift coefficients below $0{\cdot}10$.

The drag results have also been analysed in terms of a lift-dependent drag factor† $\{\pi A(C_D - C'_{D0})/C_L^2\}$. The variations of this factor with C_L for the three wings are compared in Figs. 27a to d at Mach numbers of $0{\cdot}4$, $0{\cdot}7$, $0{\cdot}9$, $0{\cdot}98$, $1{\cdot}42$, $1{\cdot}61$, $1{\cdot}82$ and $2{\cdot}0$. These figures also include the theoretical values of this factor as given, at supersonic speeds, by not-so-slender theory[2,5]. It will be seen that the induced-drag factor of wing 3 is equal to, or less than, the theoretical value, although the theoretical value only applies near $C_L = 0{\cdot}05$ where the flow is attached. The experimental factor for wing 2 is always higher than the theoretical value at the design point ($C_L = 0{\cdot}1$), but it drops below the design value at lift coefficients above $0{\cdot}2$. The differences in shape of the curves at low values of C_L for the various wings are associated with the relative positions, and shapes, of the drag polars as shown in Fig. 25.

In Fig. 28 the zero-lift drag of the plane wing is compared with theoretical estimates. The skin-friction drag was calculated by a strip method[1] based on a flat-plate turbulent boundary layer. The wave drag at supersonic speeds was calculated by slender-body theory; two values are given in Fig. 28; the upper corresponds to the wave drag of the wing alone, i.e., ignoring the small body at the rear of wing, while the lower curve includes the effect of this body (with zero base drag). When allowance is made for form drag it will be seen that agreement between the estimated and measured drags is good throughout the speed range.

---

* Note that, for convenience of presentation, different vertical scales are used in Figs. 23 and 24.

† C'_{D0} is equal to the zero-lift drag of the uncambered wing together with an increment to allow for the greater wetted areas of the cambered wings. For wing 2 the increment was $0{\cdot}0006$, and for wing 3, $0{\cdot}0003$.

3.3. *Effect of Change in Wing Shape.*

In this section the results on wings 3 and 4 are compared. It will be recalled that these two wings have the same local incidence distribution, but that this incidence distribution has been integrated to produce two wing shapes (*see* Section 2.1 and Fig. 4). On wing 3 the trailing edge is straight and all spanwise sections have drooped leading edges; on wing 4 spanwise sections forward of 0·8 of the root chord have drooped edges, but aft of this point the tips turn up.

The variations of C_L with α, C_m with C_L and C_D with C_L for the two wings are presented in Figs. 29, 30 and 31. Figs. 29 and 30 show that near the design condition ($C_L = 0{\cdot}05$), where the flow is attached, the lift and pitching moments of the two wings are similar, although wing 4 has slightly less lift; this lower lift corresponds to an increase of about 0·15° in the zero-lift angle of wing 4 as compared with wing 3. Away from the design point the lift develops less rapidly and the increase in stability with increase in C_L is less on wing 4 than on wing 3. Oil-flow patterns on wing 4 did not, however, show any significant differences to those on wing 3 (Figs. 9a and b). In spite of this, the vortex may be weaker on wing 4, or the wing shape may be less efficient in converting the low pressures associated with the vortex into lift.

The differences in the drag results are, in general, consistent with the lower non-linear lift of wing 4; that is wing 4 produces a given lift at a higher incidence than wing 3, and so has greater drag due to lift. Near the design lift coefficient the drags of the two wings are identical at supersonic speeds, but wing 4 has a slightly higher drag at subsonic speeds; it is thought that this increase in drag is due to slight differences in the transition fixing on the two wings.

These results show that large changes in wing shape, without changes in local incidence distribution, do not produce significant effects on the overall forces when the flow is attached. However, in the present case the wing with the straight trailing edge develops more non-linear lift.

3.4. *Low-Speed, High-Incidence, Results for Wings 3 and 4.*

A comparison of the results for wings 1 and 2 at $M = 0{\cdot}4$ with Keating's low-speed results[3] for equivalent wings gave excellent agreement. It was thus decided to dispense with low-speed models of wings 3 and 4, and to extend the tests at $M = 0{\cdot}4$ on these two wings up to 17°. These tests could not be made in the transonic test section due to limitations on the incidence range and so they were made in the supersonic test section with a flat top wall. The results are presented in Figs. 32, 33 and 34; for comparison these figures also include results from the transonic test section up to 10° incidence.

The purpose of these tests at high incidence was twofold. (i) To check whether any undesirable features (for example, pitch-up) occurred at these high incidences. (ii) To study the non-linear lift at high incidence, since Keating found that, for given incidence, the wing with camber designed for $C_L = 0{\cdot}1$ (wing 2) had much less lift than the plane wing.

The results show that the forces develop smoothly with increase in incidence throughout the test range. They also show a rapid increase in non-linear lift, particularly for wing 3. At 15° incidence the lift coefficients for wings 3 and 4 are 0·465 and 0·425 respectively; Keating's values at this incidence were 0·50 (wing 1) and 0·37 (wing 2). Thus at these high incidences wing 3 produces nearly as much lift as wing 1 because the increased strength of the non-linear lift compensates for its positive no-lift angle (0·6°) and for the smaller range of incidence where there is positive non-linear lift.

4. *Conclusions.*

The tests on cambered gothic wings reported in Ref. 1 have been extended to include the investigation of changes in design lift coefficient, and of changes in wing shape without changes in the local incidence distribution. The results show that:

(1) The camber design is successful in that the flow is attached over the whole wing at the design incidence, and for a limited range on either side of it. The incidence range over which the flow is attached on the cambered wings appears to increase with increasing supersonic Mach number, whereas on the uncambered wing the flow separates from the leading edge at a small incidence for all Mach numbers.

(2) At any given incidence the cambered wings give less lift than the uncambered wing because of the positive no-lift angle and because positive non-linear lift does not commence until a higher incidence.

(3) At subsonic and transonic speeds the rate of growth of non-linear lift is similar on all wings, but at Mach numbers above $M = 1{\cdot}4$ the cambered wing with a design lift coefficient of $0{\cdot}05$, and a straight trailing edge, appears to develop more non-linear lift than the uncambered wing, whereas the wing with $(C_L)_d = 0{\cdot}1$ develops no non-linear lift.

(4) Camber causes a forward moment of the wing centre-of-pressure position at subsonic and transonic speeds; this shift is most marked near $M = 1{\cdot}0$. At supersonic speeds the effect of camber on centre-of-pressure position is small.

(5) Both the camber shapes designed for $C_L = 0{\cdot}05$ have slightly lower drags than the plane wing at positive C_L, but the drag of the camber designed for $C_L = 0{\cdot}10$ is greater than that of the uncambered wing at lift coefficients below about $0{\cdot}1$ at subsonic speeds and $0{\cdot}15$ at supersonic speeds.

(6) Changes in spanwise camber, without changes in the camber incidence distribution, do not alter the force characteristics when the flow is attached, but with separated flow the wing with the straight trailing edge develops the most non-linear lift.

LIST OF SYMBOLS

A — Aspect ratio

$c(y)$ — Local chord

c_0 — Root chord

$\bar{c}$ — Mean aerodynamic chord

$$= \int_{-s_T}^{s_T} c^2(y)dy \Big/ \int_{-s_T}^{s_T} c(y)dy$$

C_L — Lift coefficient = Lift/qS

C_D — Drag coefficient = Drag/qS

$(C_D)_0$ — Drag coefficient of plane wing at zero lift

C_m — Pitching-moment coefficient = Pitching moment/$qS\bar{c}$ (referred to quarter-chord point of the mean aerodynamic chord)

$\bar{C}_L$, $\bar{C}_m$ — Lift and pitching-moment coefficients at minimum lift-curve slope (*see* Section 3.2.1)

M — Free-stream Mach number

q — Free-stream dynamic pressure

S — Wing area

$S(x)$ — Cross-sectional area distribution

s_T — Semi-span at trailing edge

$s(x)$ — Equation of leading edge (local semi-span)

α — Wing incidence: incidence of uncambered centre section of cambered wings

$\bar{\alpha}$ — Incidence at minimum lift-curve slope

REFERENCES

No.	*Author*	*Title, etc.*
1	L. C. Squire	An experimental investigation at supersonic speeds of the characteristics of two gothic wings, one plane and one cambered. A.R.C. R. & M. 3211. May, 1959.
2	J. Weber	Design of warped slender wings with the attachment line along the leading edge. Unpublished M.o.A. Report.
3	R. F. A. Keating	Low-speed wind-tunnel tests on sharp-edged gothic wings of aspect ratio 3/4. A.R.C. C.P. 576. May, 1960.
4	E. C. Maskell	Flow separations in three dimensions. A.R.C. 18,063. November, 1955.
5	MacC. Adams and W. R. Sears ..	Slender-body theory—review and extension. *J. Ae. Sci.* Vol. 20. No. 2. February, 1953.
6	L. C. Squire	Some applications of 'not-so-slender' wing theory to wings with curved leading edges. A.R.C. R & M 3278. July, 1960.
7	J. H. B. Smith	A theory of the separated flow from the curved leading edge of a slender wing. A.R.C. R. & M. 3116. November, 1957.

TABLE 1

Details of Models

Dimensions (all models)

Planform	$y = s(x) = s_T \frac{x}{c_0}\left(2 - \frac{x}{c_0}\right)$
Centre-line chord (c_0)	20 inches
Span ($2s_T$)	10 inches
Aerodynamic mean chord ($\bar{\bar{c}}$)	15 inches
Area (S)	133·3 square inches
Distance of $\frac{\bar{\bar{c}}}{4}$ aft of apex	8·75 inches
Volume ($= 0{\cdot}009c_0^3$)	72 cubic inches

Thickness distribution (without sting fairing)

Area distribution

$$S(x) = 100{\cdot}8\left(\frac{x}{c_0}\right)^2\left\{1-\left(\frac{x}{c_0}\right)\right\}\left\{1-\frac{3}{2}\left(\frac{x}{c_0}\right)+\left(\frac{x}{c_0}\right)^2-\frac{1}{4}\left(\frac{x}{c_0}\right)^3\right\} \text{ square inches.}$$

Centre-line semi-thickness

$$\frac{z}{c_0} = 0{\cdot}126\left(\frac{x}{c_0}\right)\left\{1-\left(\frac{x}{c_0}\right)\right\}\left\{2-2\left(\frac{x}{c_0}\right)+\left(\frac{x}{c_0}\right)^2\right\}.$$

Camber distribution (Ref. 2)

On all the cambered wings the local incidence distribution is given by

$$\frac{\partial z}{\partial x} = \text{C (constant) for } 0 < |\eta| \leqslant \eta_0(x)$$

$$= C\left[1 - \frac{\pi(|\eta|-\eta_0)^2}{(1+2\eta_0^2)\cos^{-1}\eta_0 - 3\eta_0\sqrt{(1-\eta_0^2)}}\right] \text{ for } \eta_0(x) \leqslant |\eta| < 1,$$

where

$$\eta = y/s(x) \qquad \eta_0(x) = \frac{0{\cdot}8}{2-(x/c_0)}.$$

The constant C is equal to 0·0956 for wing 2 and 0·0478 for wings 3 and 4.

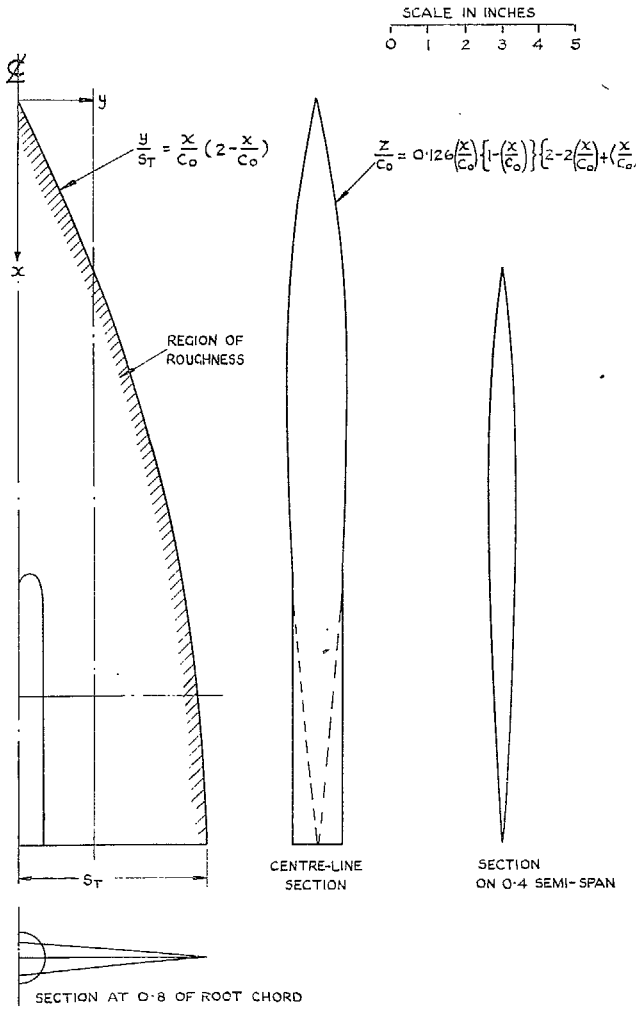

FIG. 1. Details of plane wing (wing 1).

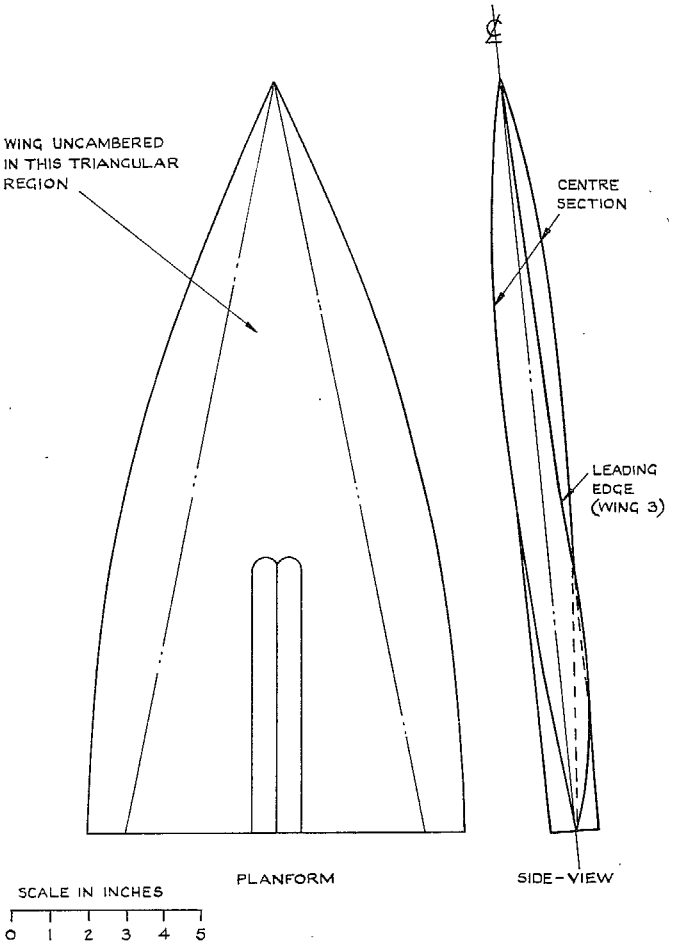

FIG. 2. Details of the camber design.

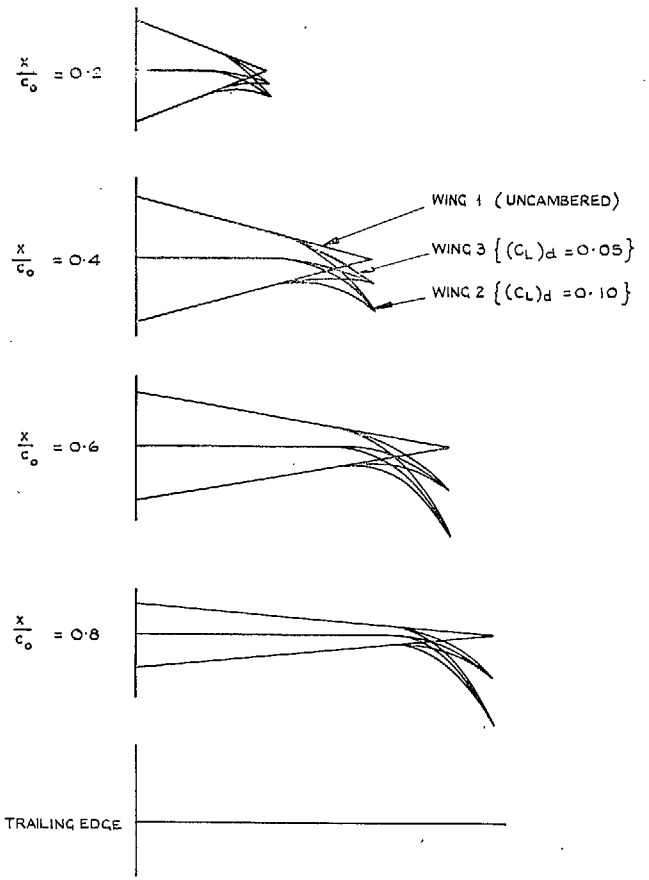

FIG. 3. Details of wing cross-sections: wings 1, 2 and 3.

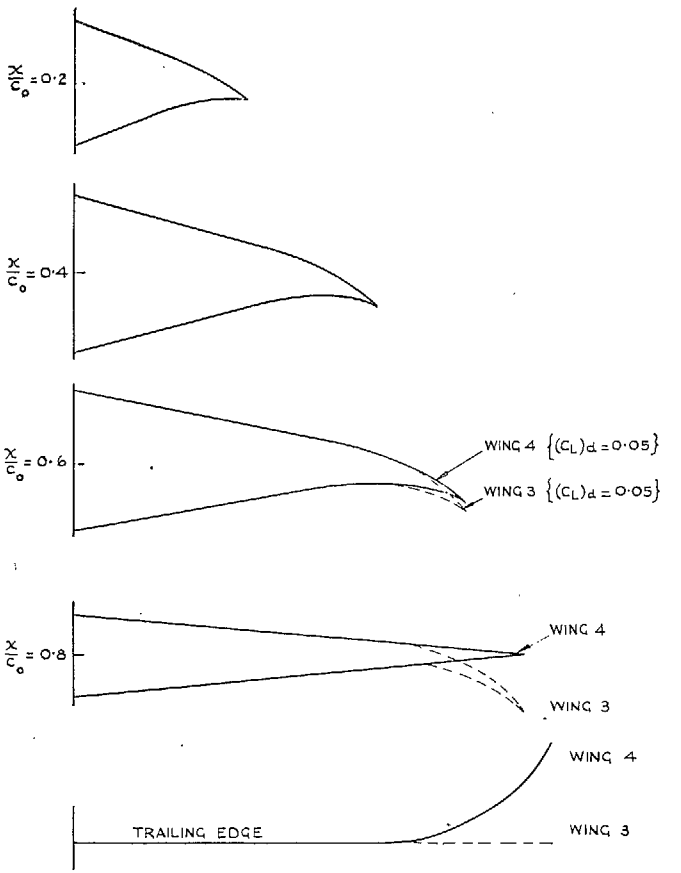

FIG. 4. Details of wing cross-sections: wings 3 and 4.

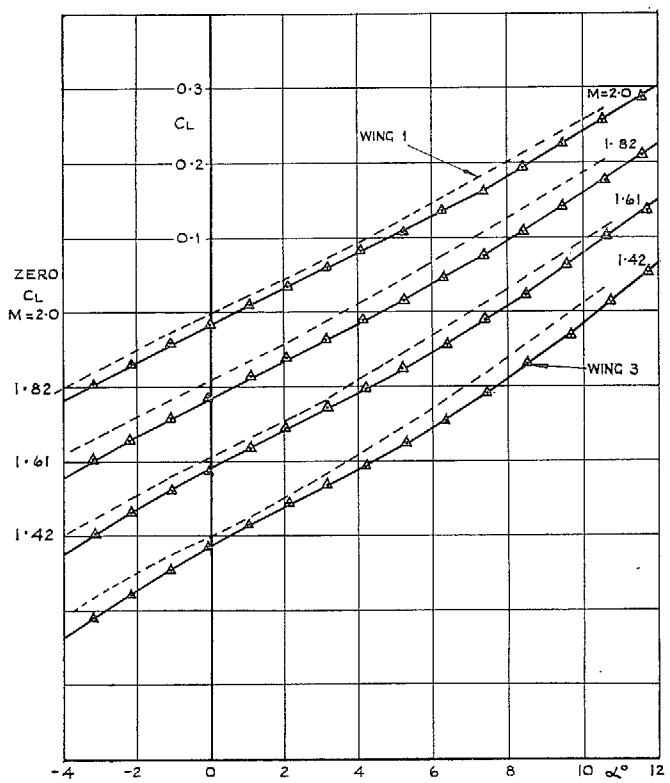

FIG. 5. Variation of C_L with α: wings 1 and 3.

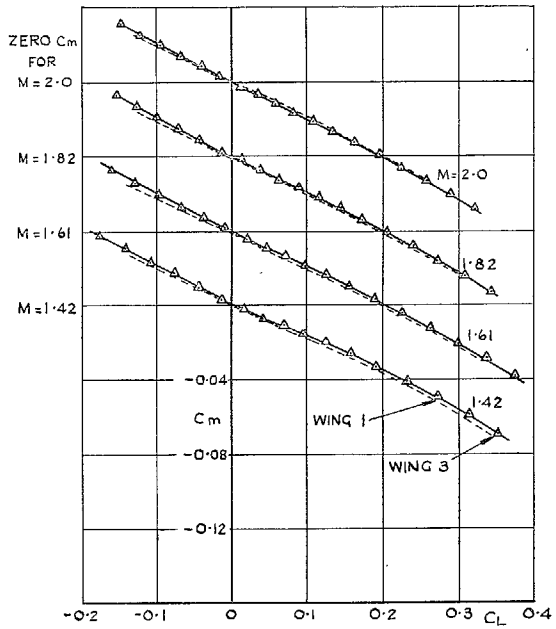

FIG. 6. Variation of C_m with C_L: wings 1 and 3.

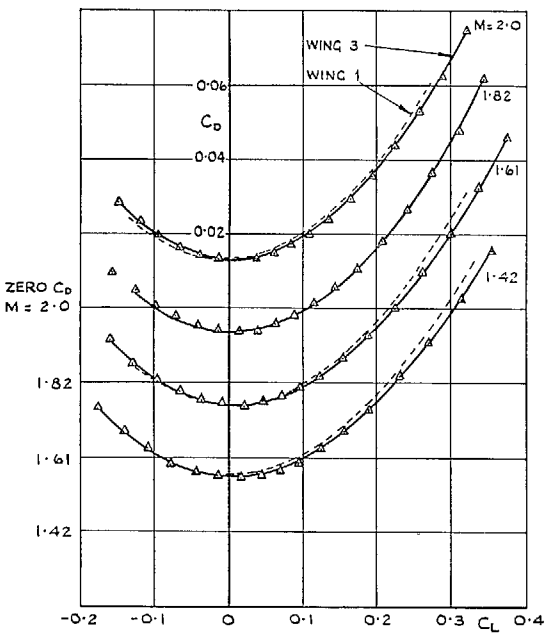

FIG. 7. Variation of C_D with C_L: wings 1 and 3.

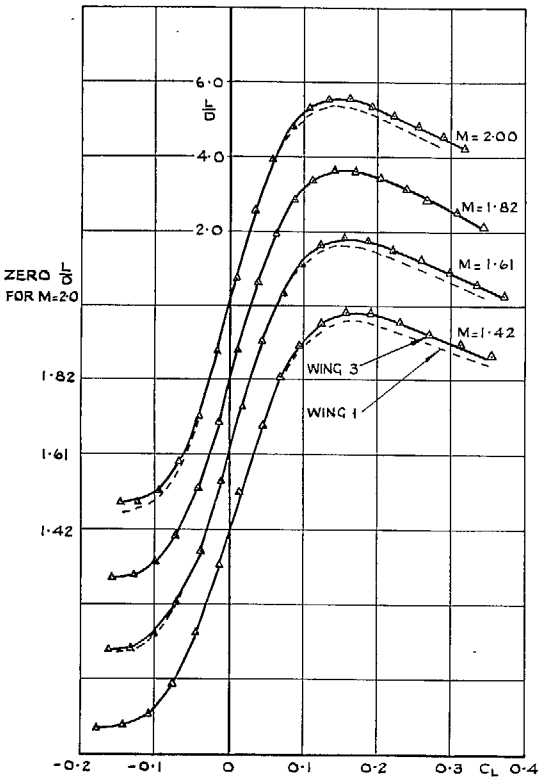

FIG. 8. Variation of L/D with C_L: wings 1 and 3.

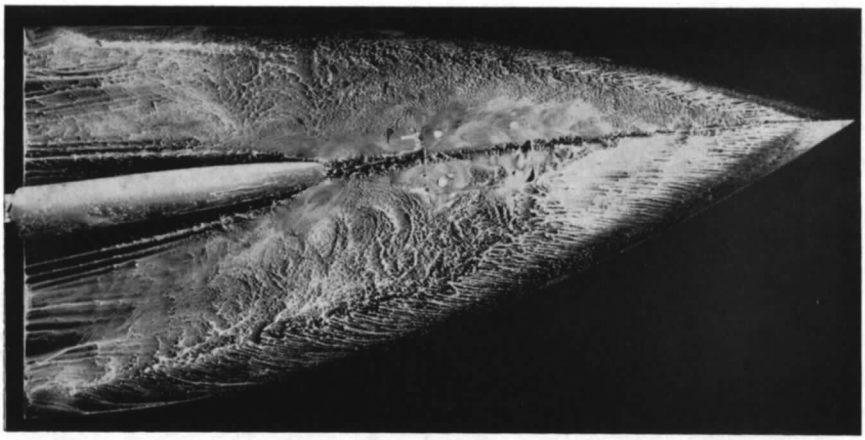

$\alpha = 3.1^{\circ}$: Upper surface $C_L = 0.070$

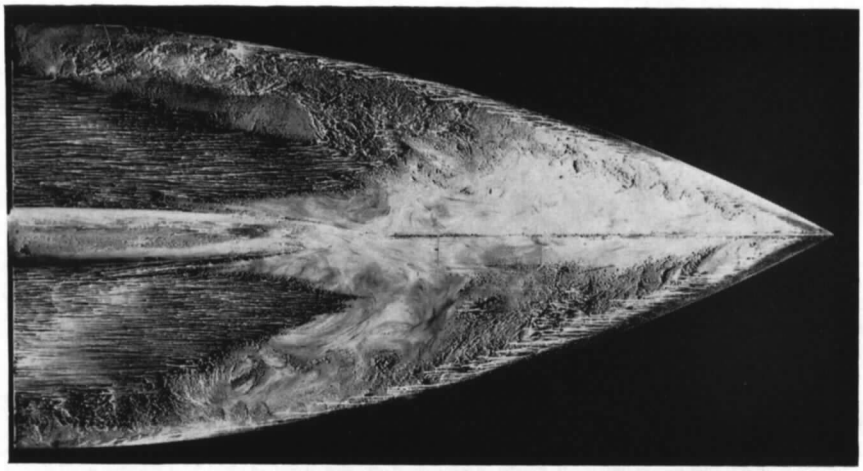

$\alpha = 3.1^{\circ}$: Lower surface $C_L = 0.070$

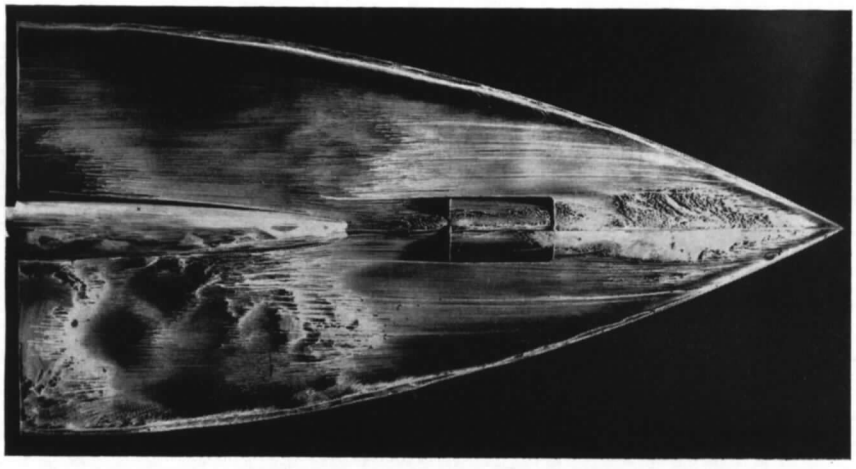

$\alpha = 0$: Lower surface $C_L = -0.010$

FIG. 9a. Oil-flow photographs. Wing 3. $M = 1{\cdot}61$.

$\alpha = 8.4^{\circ}$: Upper surface $C_L = 0.223$

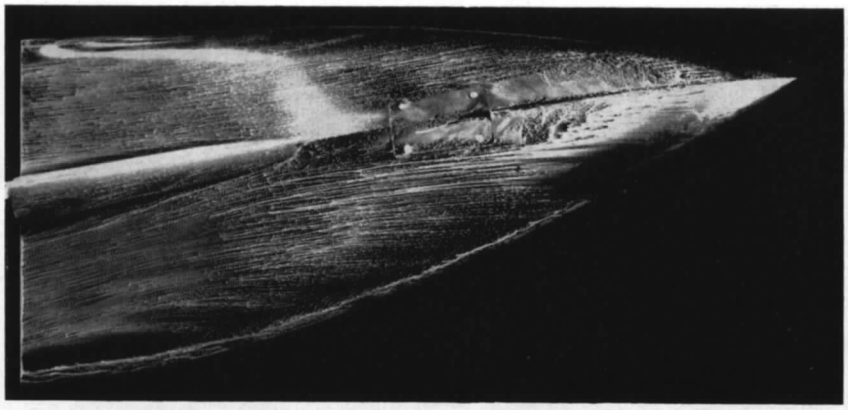

$\alpha = 6.3^{\circ}$: Upper surface $C_L = 0.155$

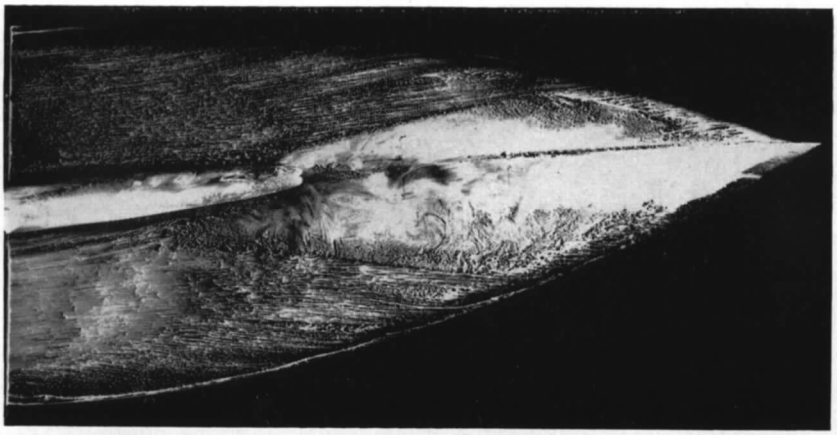

$\alpha = 4.2^{\circ}$: Upper surface $C_L = 0.097$

FIG. 9b. Oil-flow photographs. Wing 3. $M = 1{\cdot}61$.

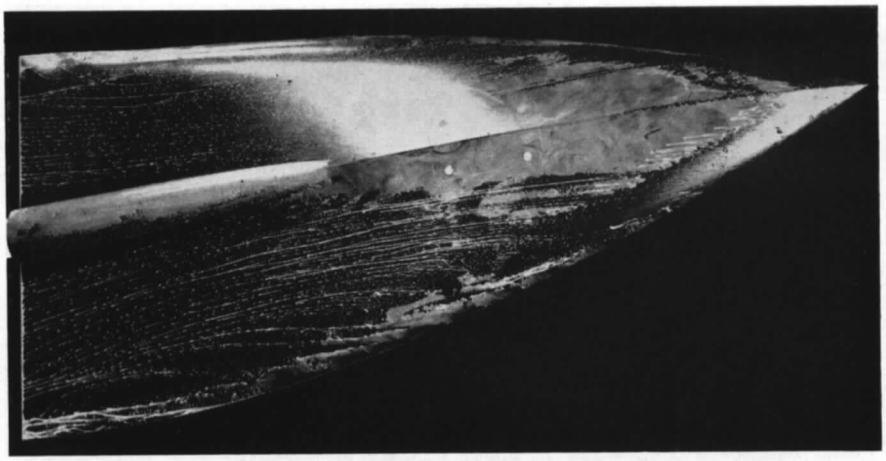

$\alpha = 8.4^{\circ}$: Upper surface $C_L = 0.193$

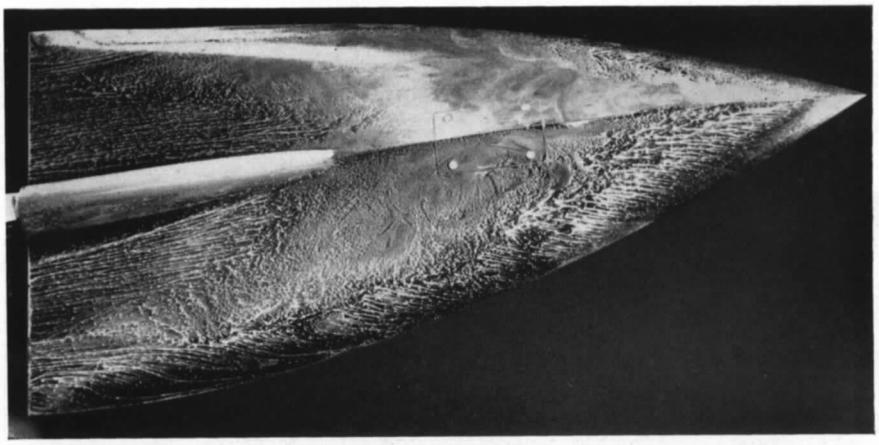

$\alpha = 4.2^{\circ}$: Upper surface $C_L = 0.082$

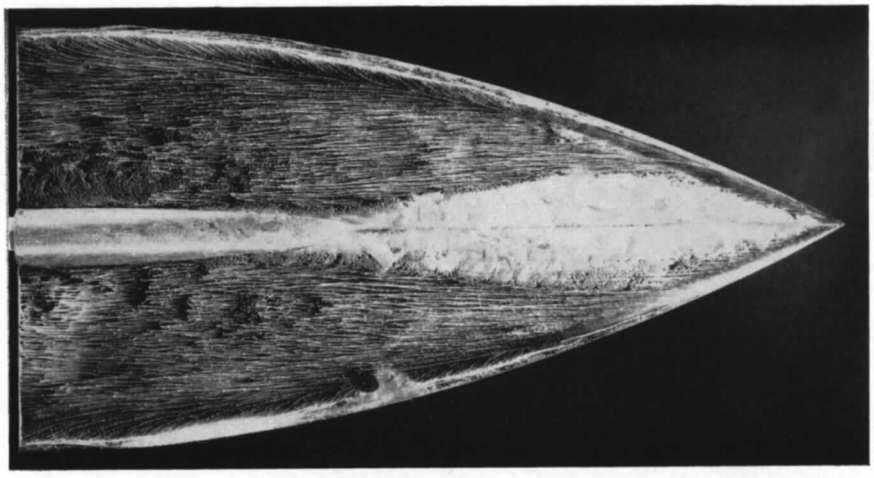

$\alpha = 0^{\circ}$: Lower surface $C_L = -0.015$

FIG. 10. Oil-flow photographs. Wing 3. $M = 2{\cdot}0$.

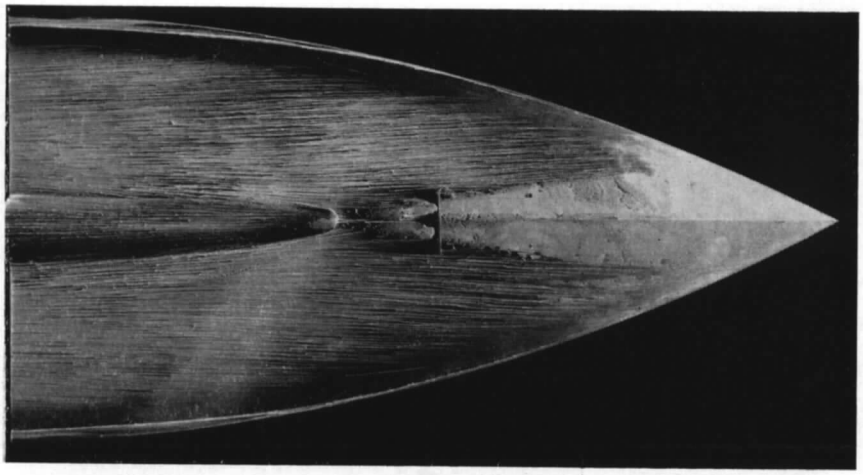

M = 1.61

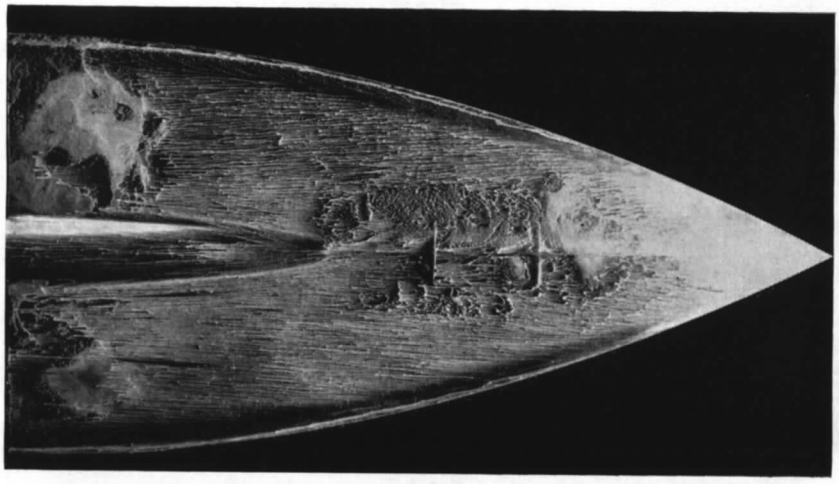

M = 2.0

FIG. 11a. Oil-flow photographs. Wing 1. $\alpha \doteqdot 2°$.

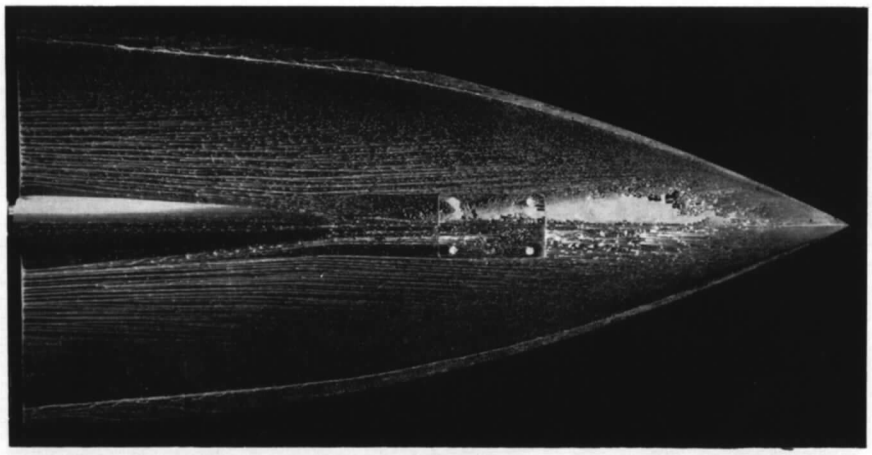

M = 1.61

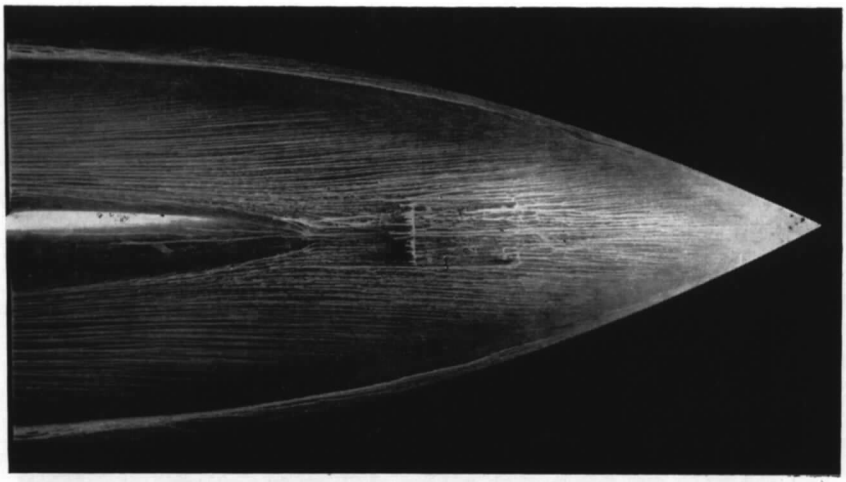

M = 2.0

FIG. 11b. Oil-flow photographs. Wing 1. $\alpha \doteqdot 4°$.

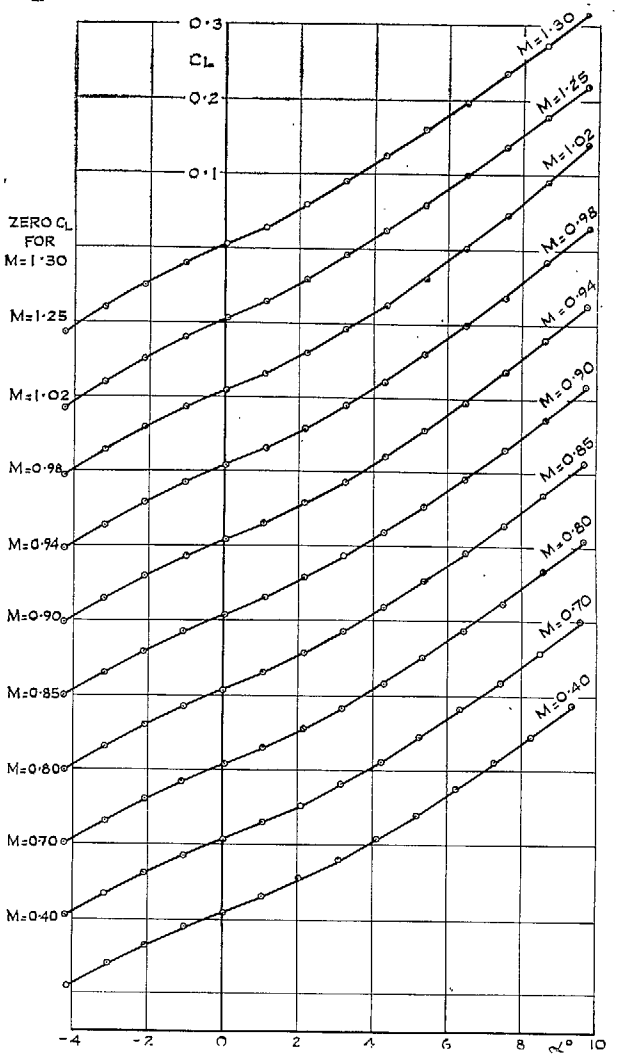

FIG. 12. Variation of C_L with α: Wing 1.

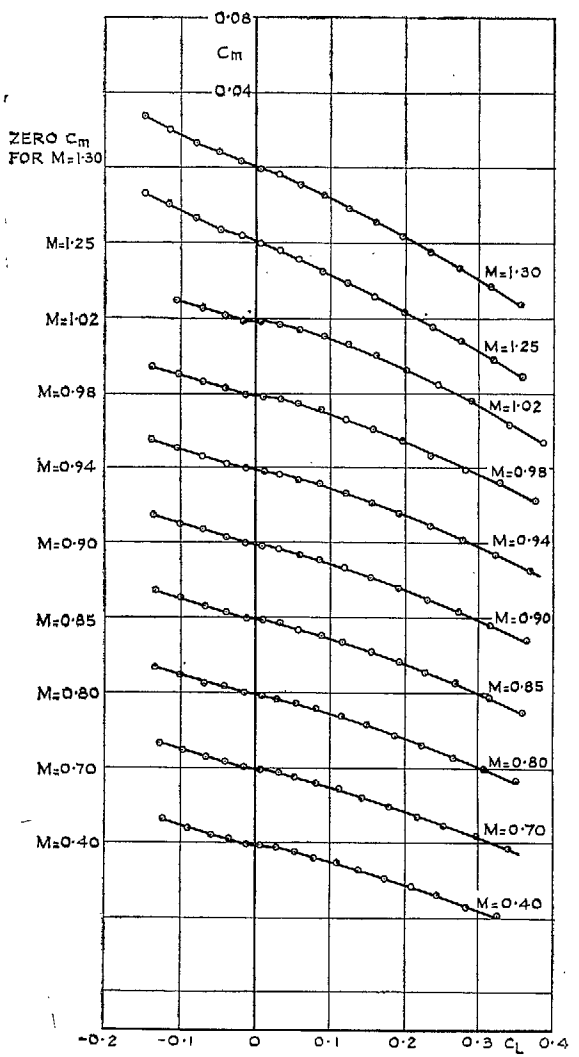

FIG. 13. Variation of C_m with C_L: wing 1.

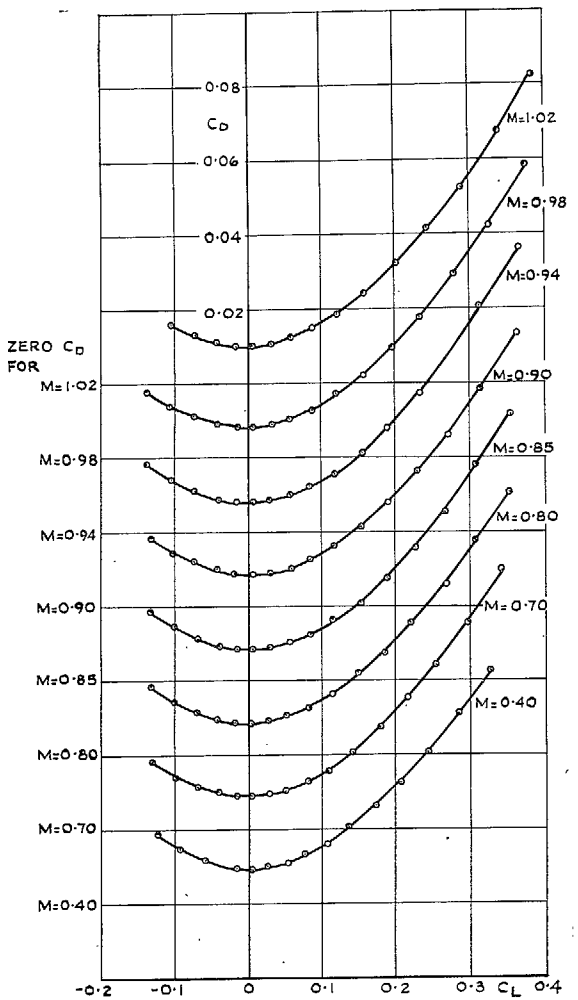

FIG. 14. Variation of C_D with C_L: wing 1.

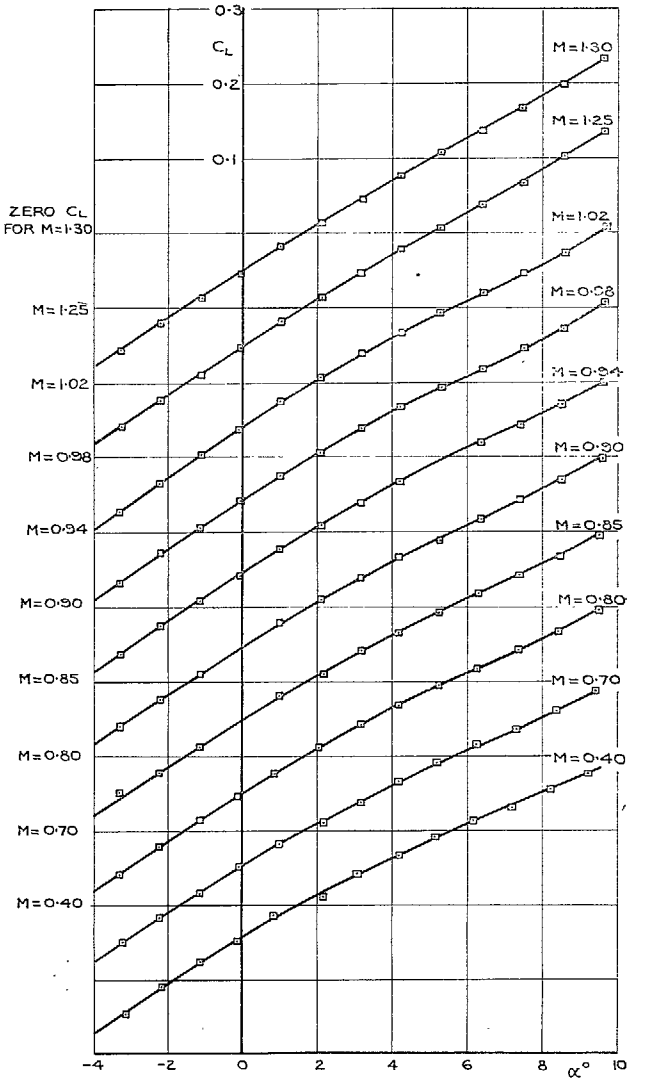

FIG. 15. Variation of C_L with α: wing 2.

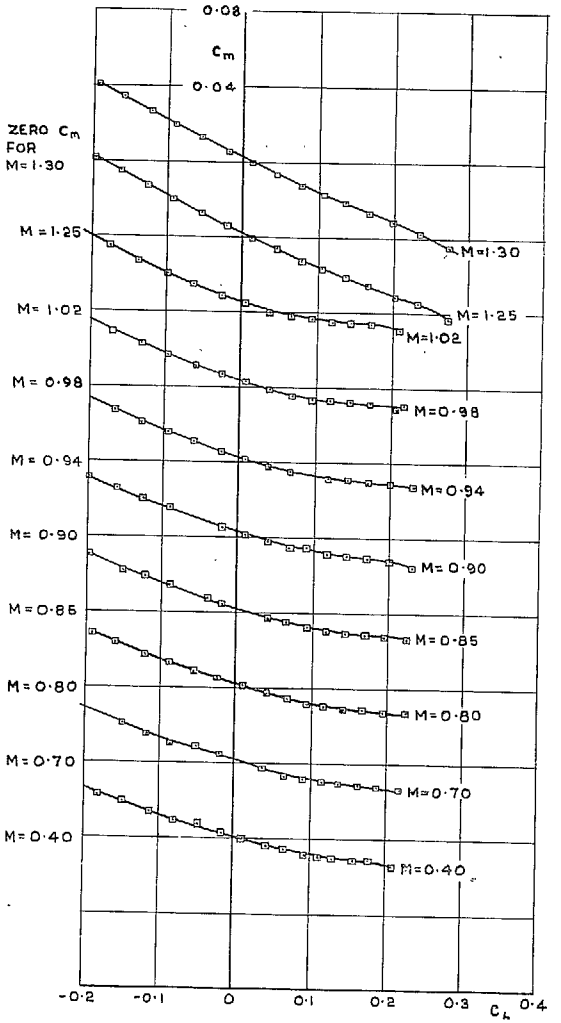

FIG. 16. Variation of C_m with C_L: wing 2.

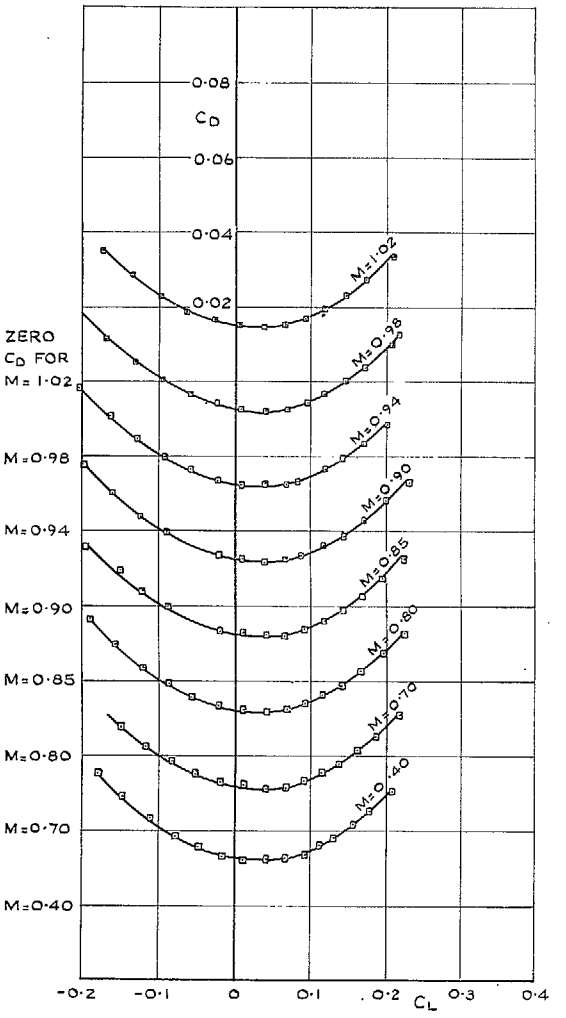

FIG. 17. Variation of C_D with C_L: wing 2.

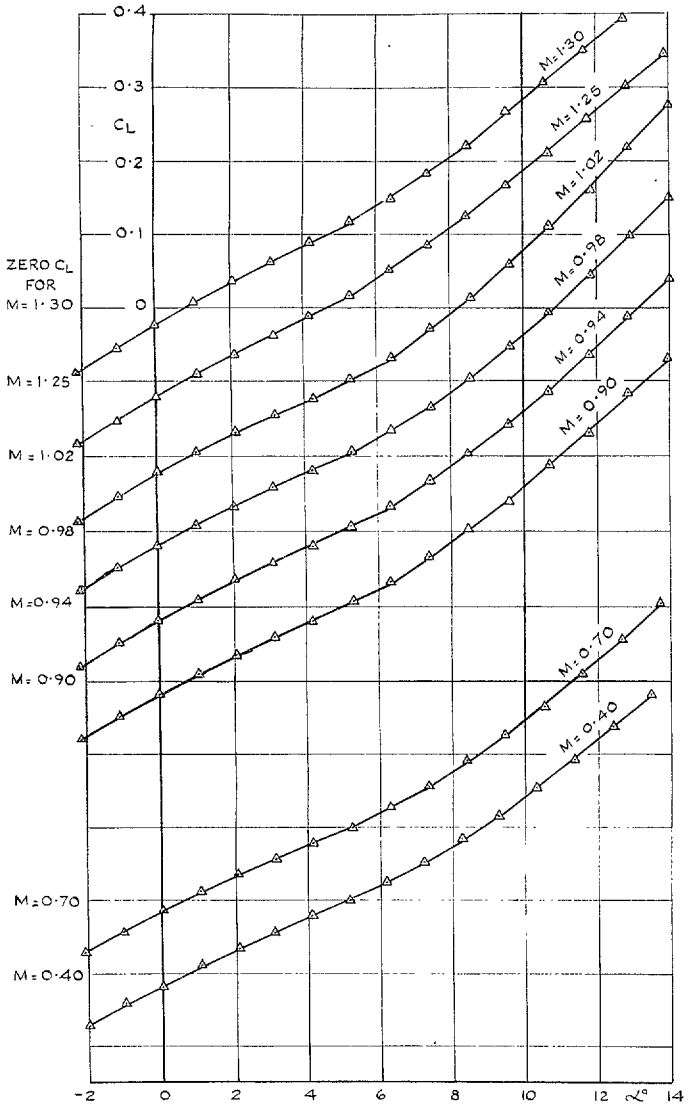

FIG. 18. Variation of C_L with α: wing 3.

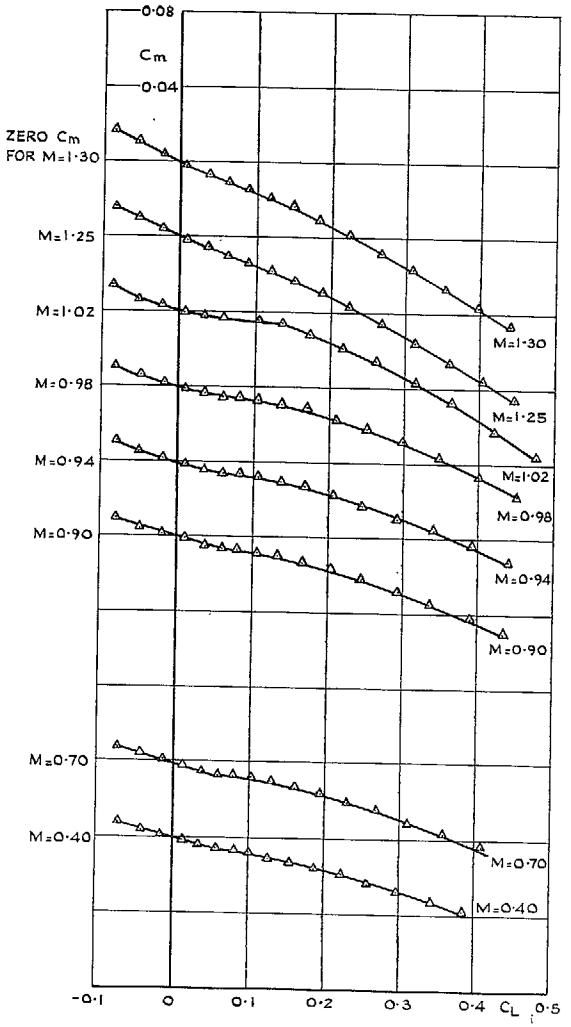

FIG. 19. Variation of C_m with C_L: wing 3.

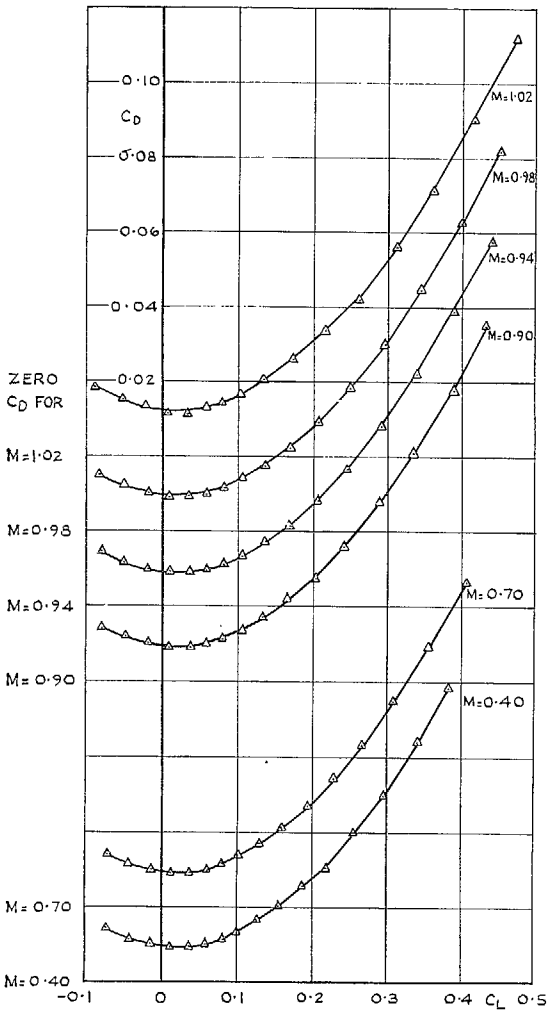

FIG. 20. Variation of C_D with C_L: wing 3.

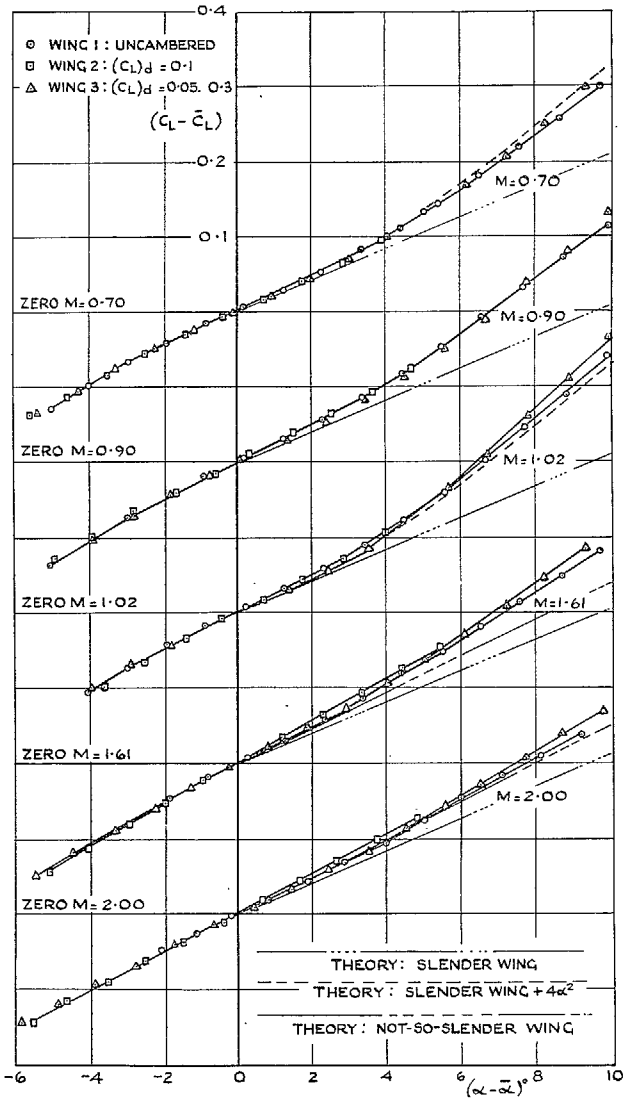

FIG. 21. Variation of $(C_L - \bar{C}_L)$ with $(\alpha - \bar{\alpha})$: wings 1, 2 and 3.

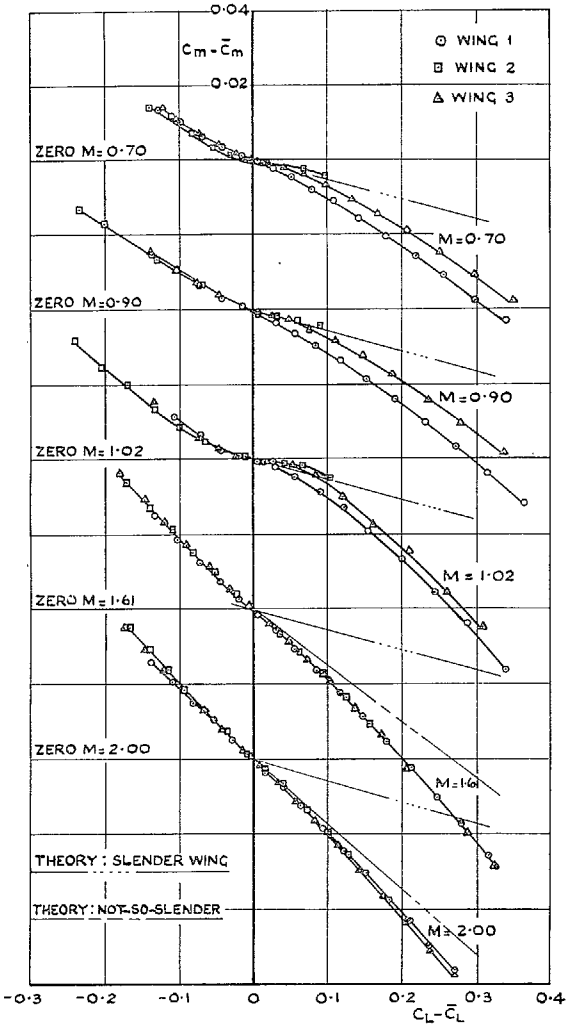

FIG. 22. Variation of $(C_m - \bar{C}_m)$ with $(C_L - \bar{C}_L)$: wings 1, 2 and 3.

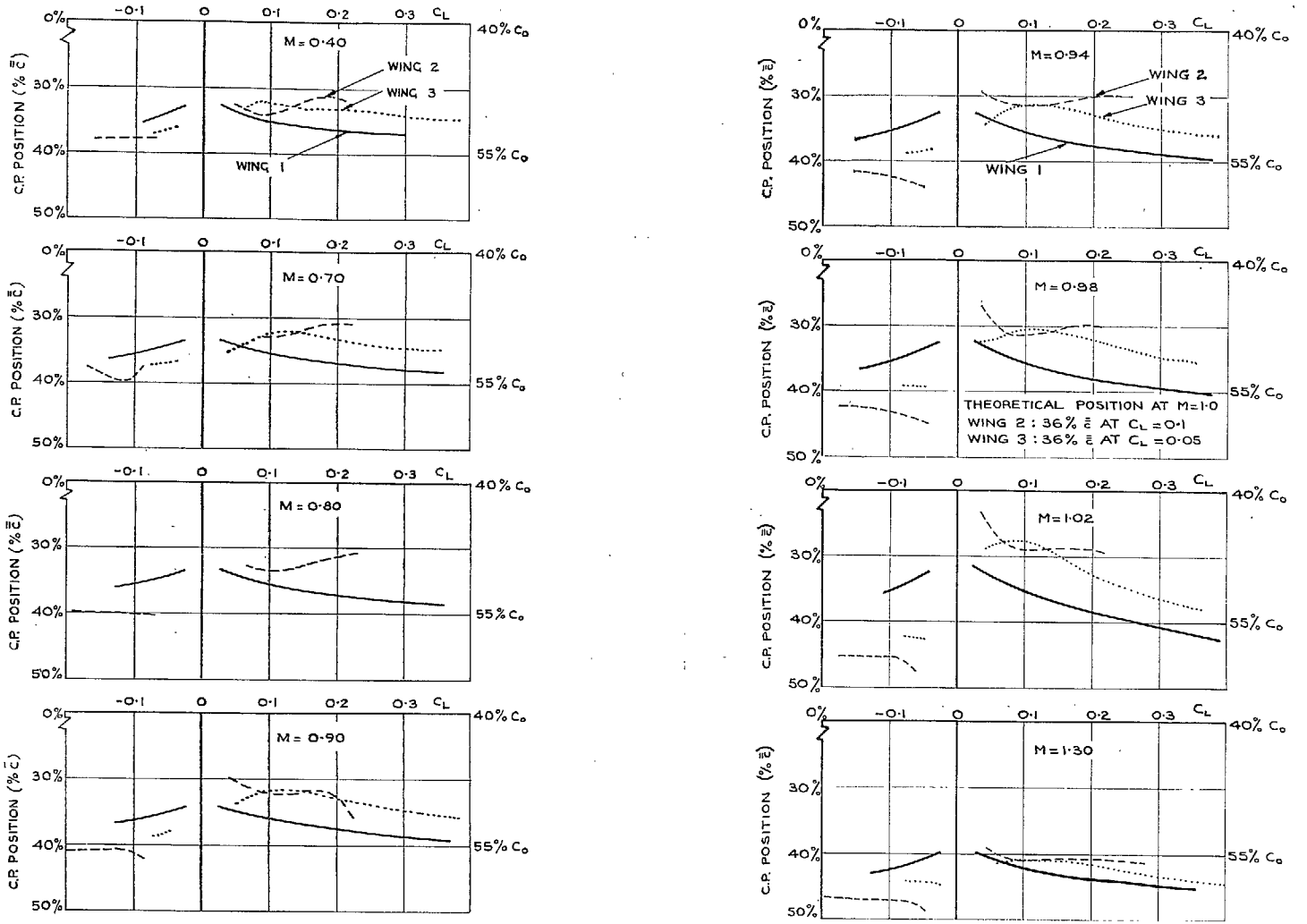

FIGS. 23a and b. Variation of centre-of-pressure position with C_L at constant Mach number: wings 1, 2 and 3.

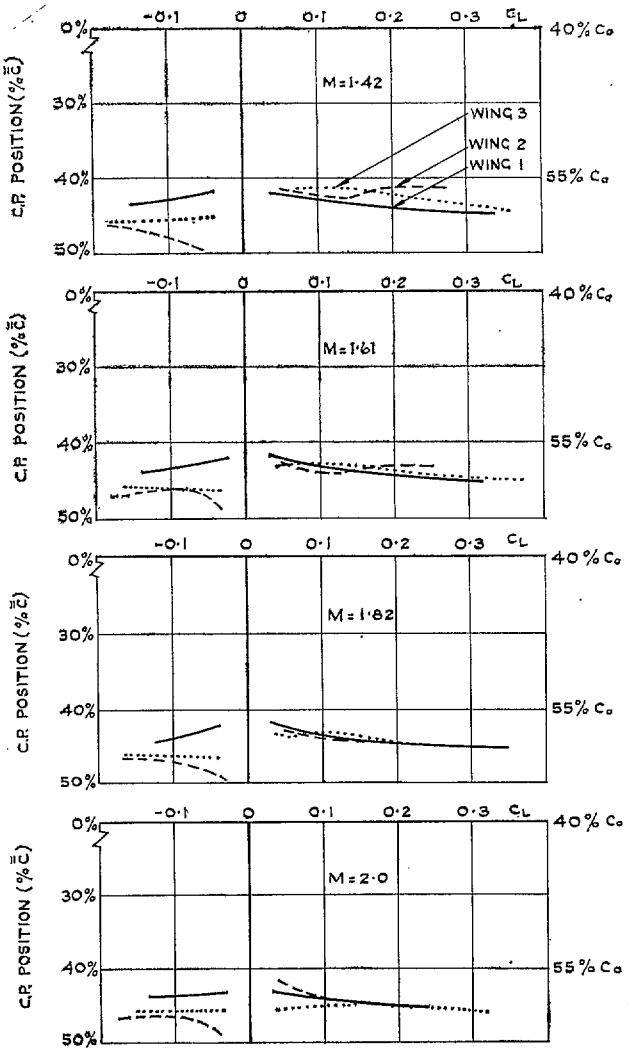

FIG. 23c. Variation of centre-of-pressure position with C_L at constant Mach number: wings 1, 2 and 3.

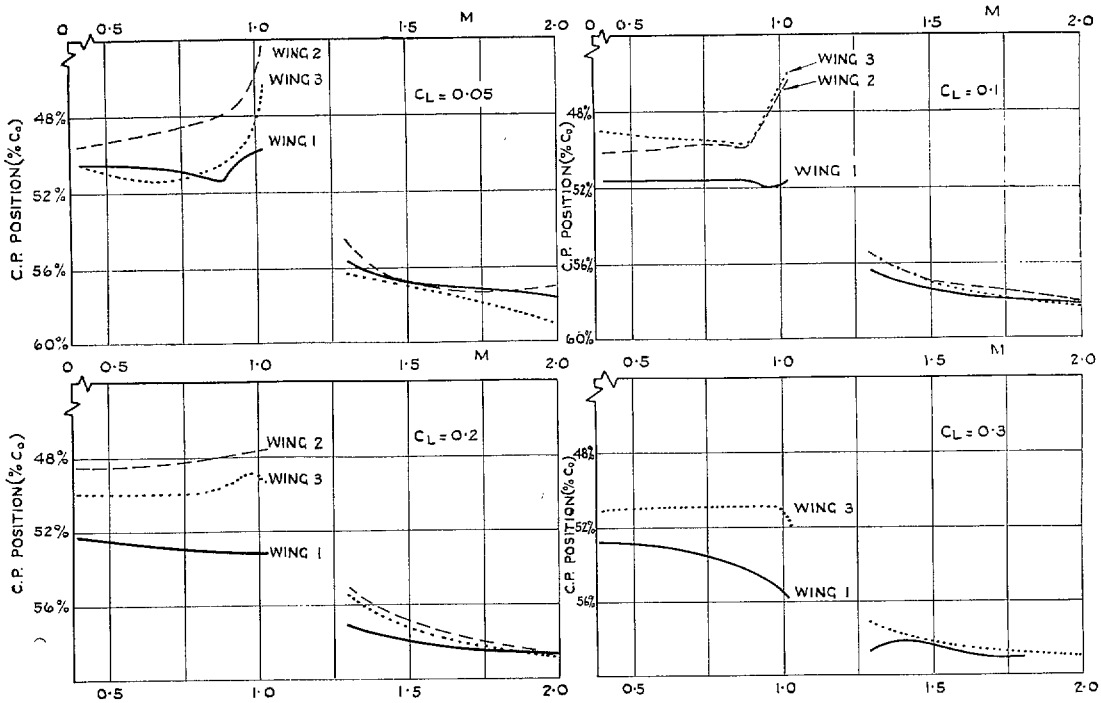

FIG. 24. Variation of centre-of-pressure with Mach number, position at fixed C_L: wings 1, 2 and 3.

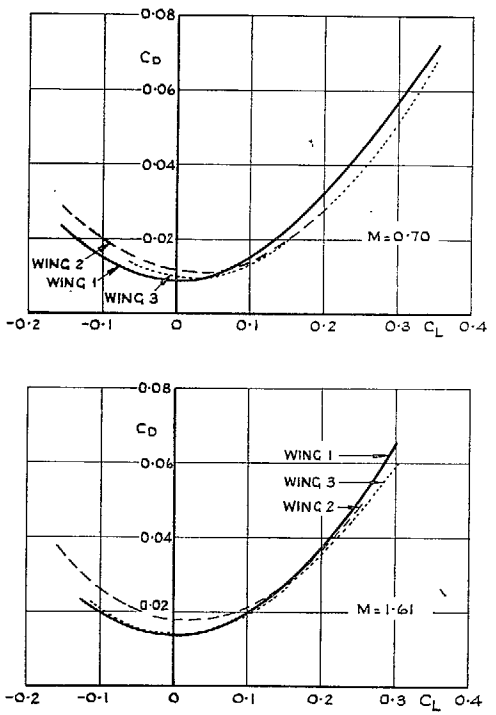

FIG. 25. Comparison of drag polars of wings 1, 2 and 3.

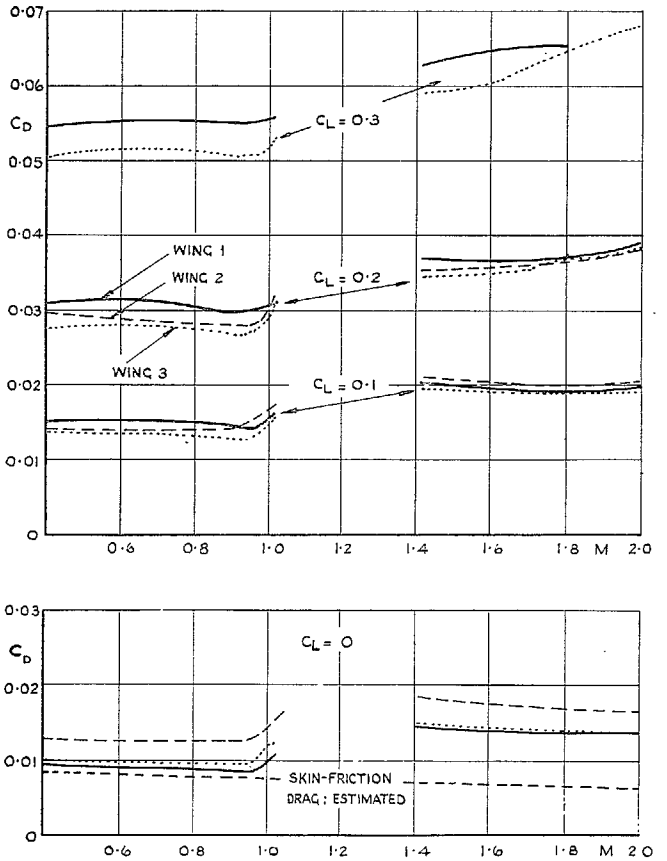

FIG. 26. Variation with Mach number of the drag at fixed C_L: wings 1, 2 and 3.

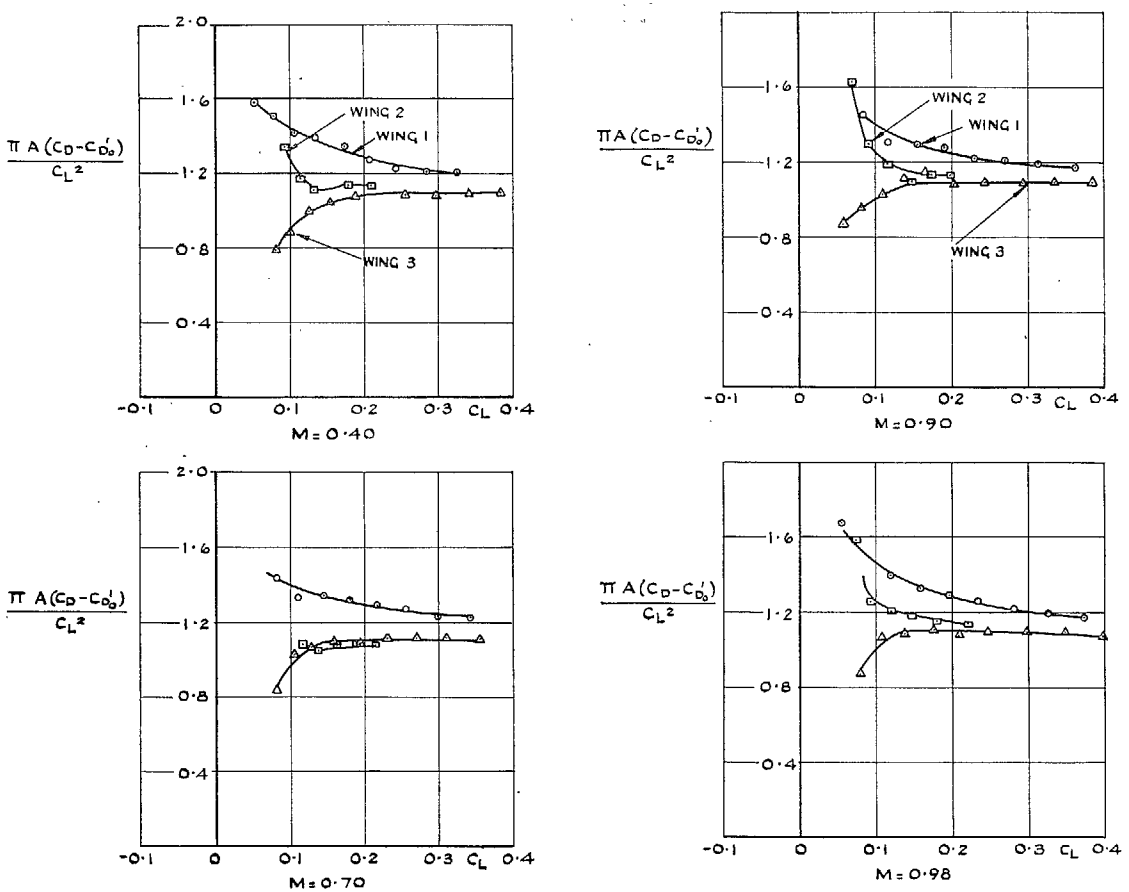

FIGS. 27a and b. Variation with C_L of the lift-dependent drag factor: wings 1, 2 and 3.

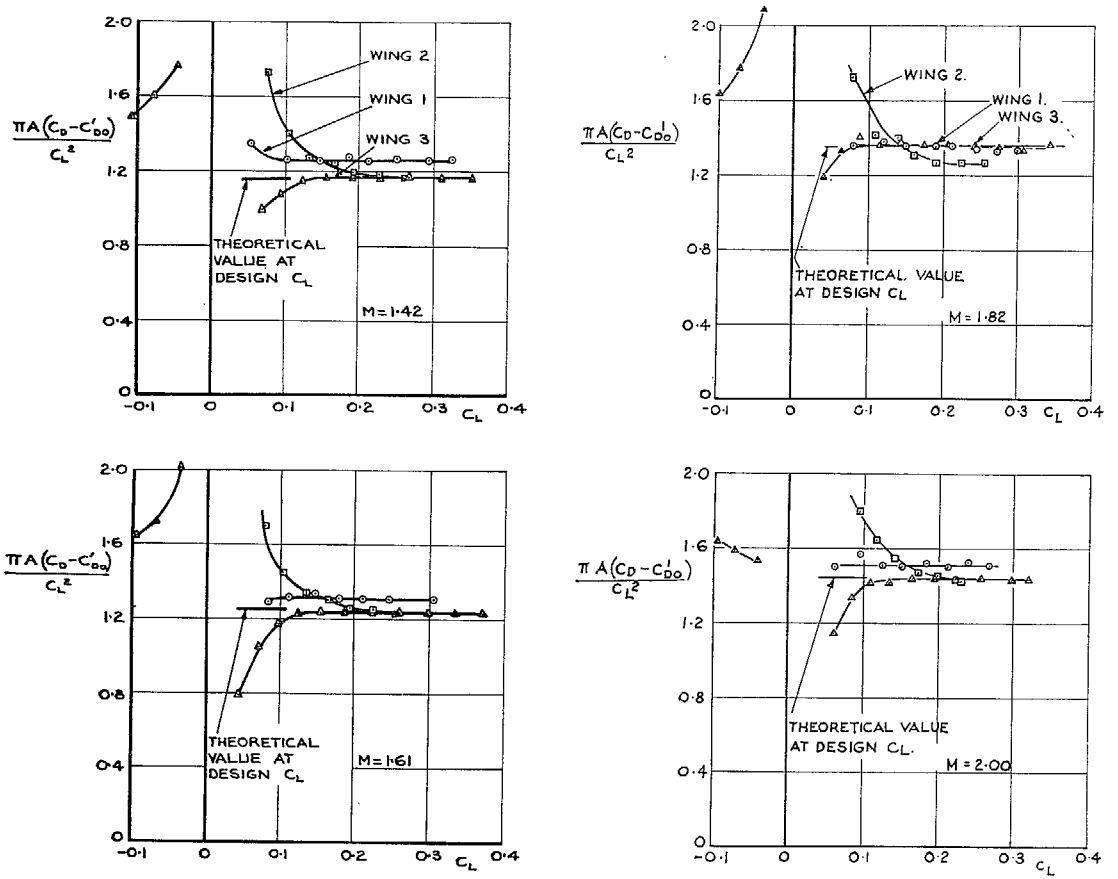

FIGS. 27c and d. Variation with C_L of the lift-dependent drag factor: wings 1, 2 and 3.

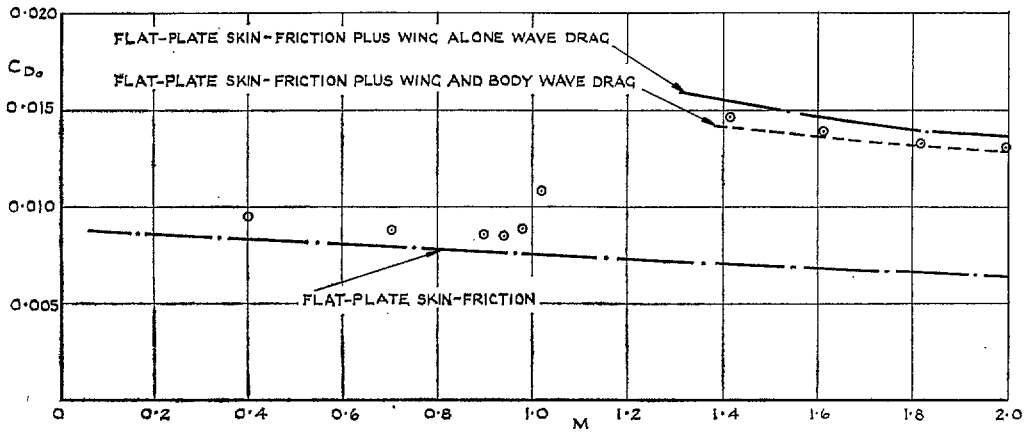

FIG. 28. Comparison of zero-lift drag of wing 1 with theory.

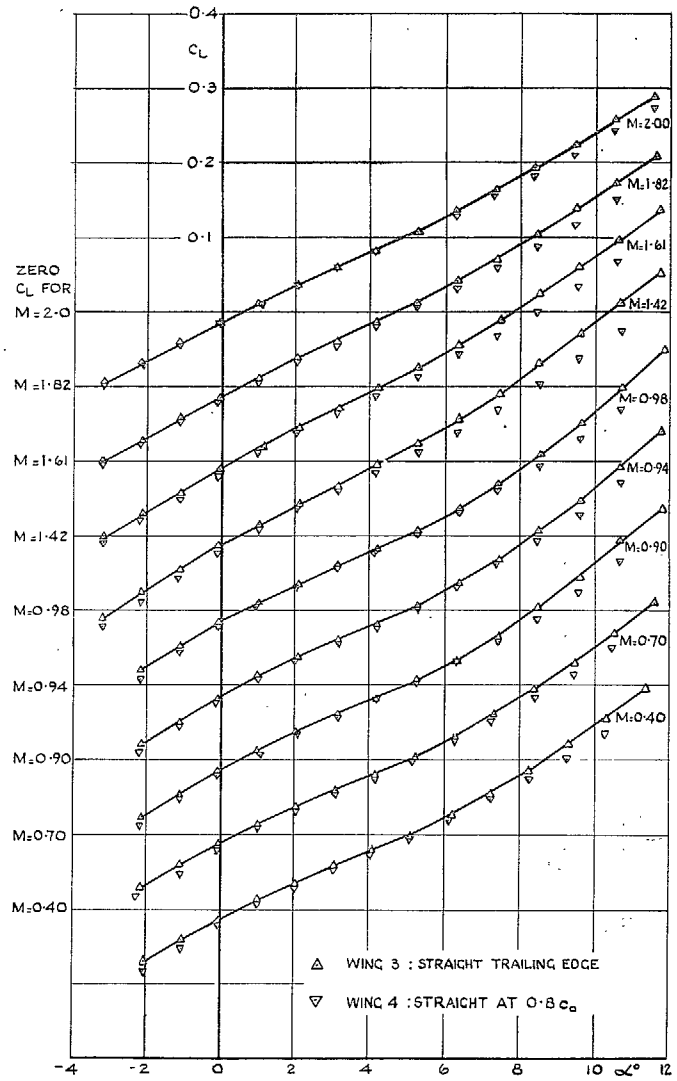

FIG. 29. Variation of C_L with α: wings 3 and 4.

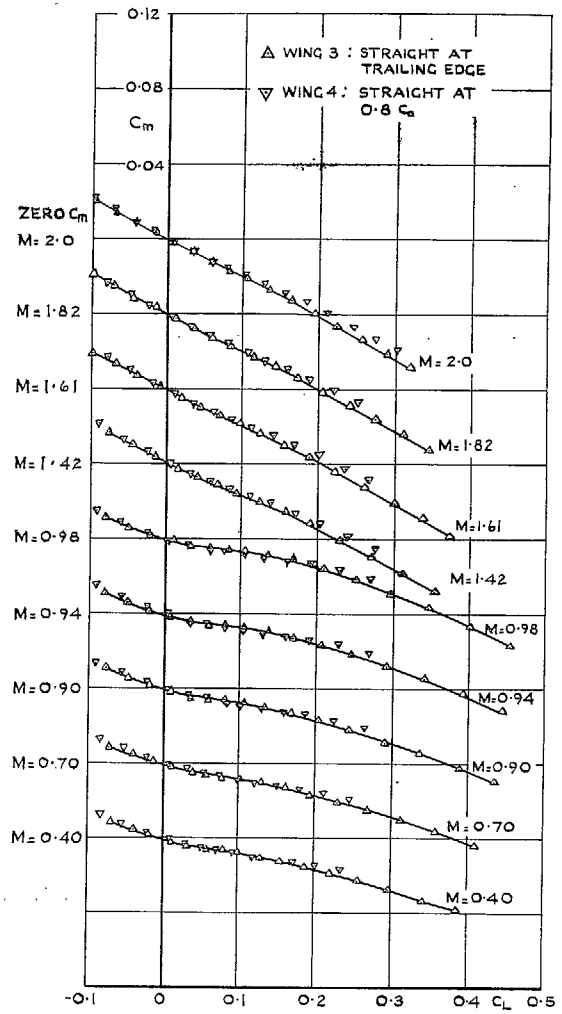

FIG. 30. Variation of C_m with C_L: wings 3 and 4.

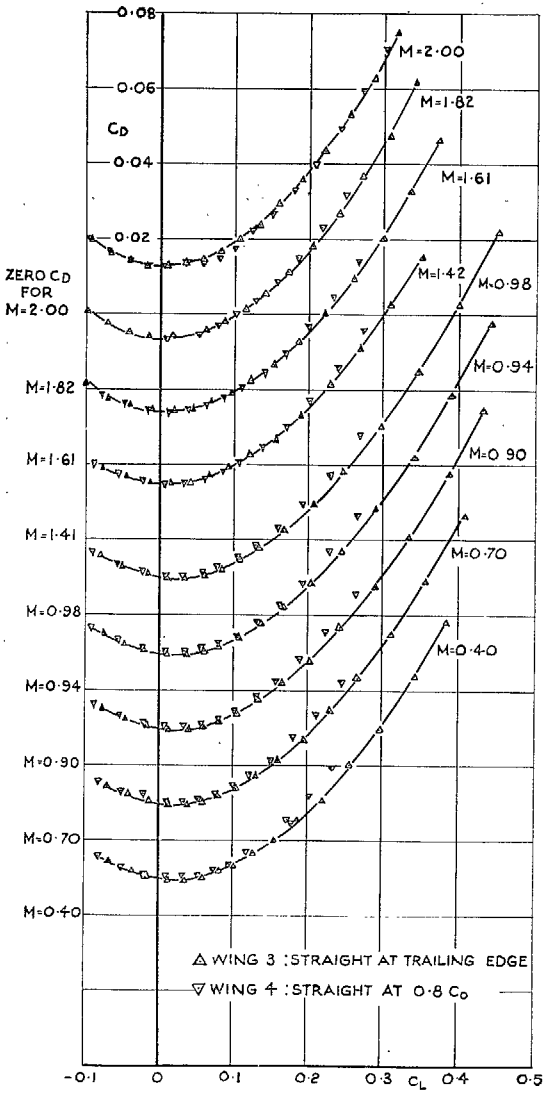

FIG. 31. Variation of C_D with C_L: wings 3 and 4.

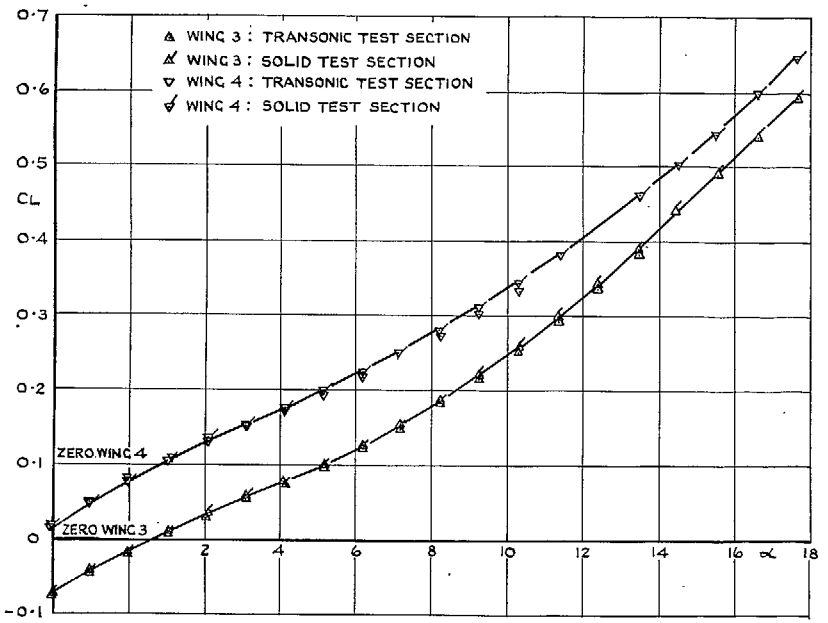

FIG. 32. Variation of C_L with α: $M = 0{\cdot}4$: wings 3 and 4.

(86513) Wt. 64/1857 K5 2/63 Hw.

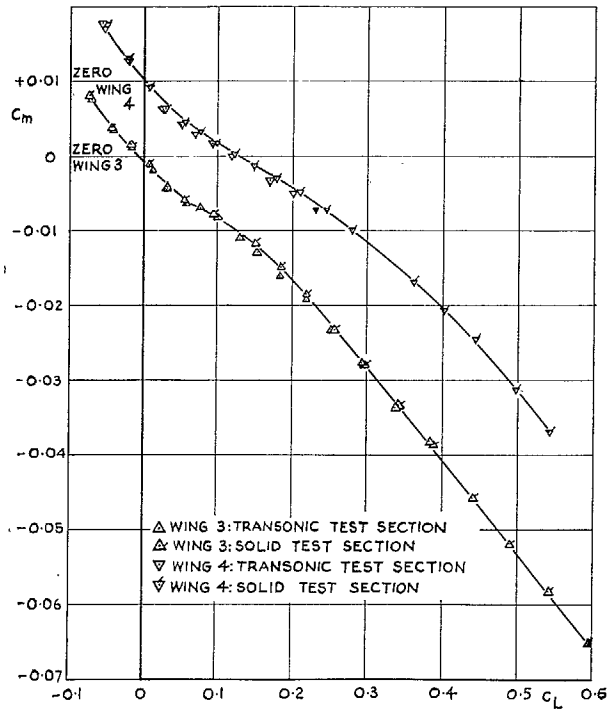

FIG. 33. Variation of C_m with C_L: $M = 0{\cdot}4$: wings 3 and 4.

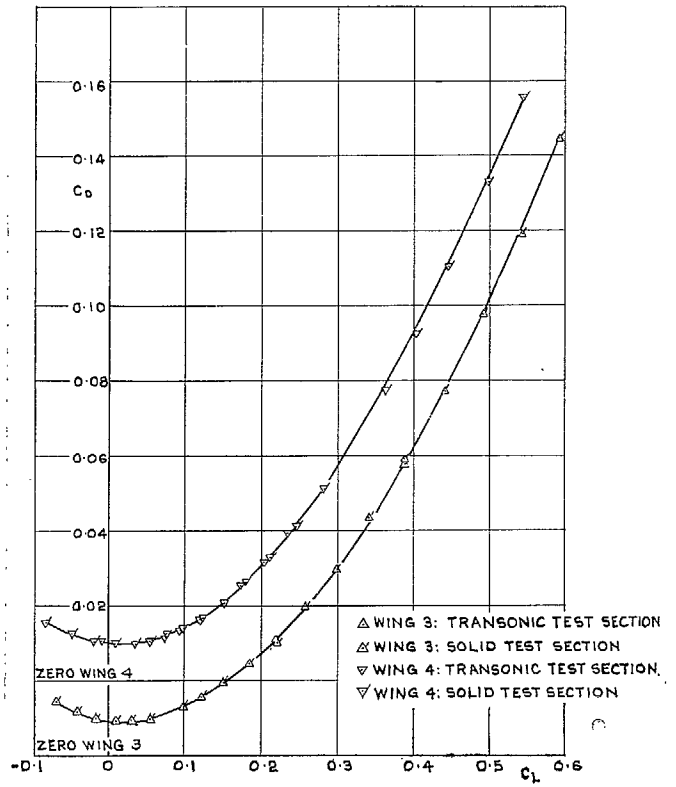

FIG. 34. Variation of C_D with C_L: $M = 0{\cdot}4$: wings 3 and 4.

Publications of the Aeronautical Research Council

ANNUAL TECHNICAL REPORTS OF THE AERONAUTICAL RESEARCH COUNCIL (BOUND VOLUMES)

1942 Vol. I. Aero and Hydrodynamics, Aerofoils, Airscrews, Engines. 75*s.* (post 2*s.* 9*d.*)
Vol. II. Noise, Parachutes, Stability and Control, Structures, Vibration, Wind Tunnels. 47*s.* 6*d.* (post 2*s.* 3*d.*)

1943 Vol. I. Aerodynamics, Aerofoils, Airscrews. 80*s.* (post 2*s.* 6*d.*)
Vol. II. Engines, Flutter, Materials, Parachutes, Performance, Stability and Control, Structures. 90*s.* (post 2*s.* 9*d.*)

1944 Vol. I. Aero and Hydrodynamics, Aerofoils, Aircraft, Airscrews, Controls. 84*s.* (post 3*s.*)
Vol. II. Flutter and Vibration, Materials, Miscellaneous, Navigation, Parachutes, Performance, Plates and Panels, Stability, Structures, Test Equipment, Wind Tunnels. 84*s.* (post 3*s.*)

1945 Vol. I. Aero and Hydrodynamics, Aerofoils. 130*s.* (post 3*s.* 6*d.*)
Vol. II. Aircraft, Airscrews, Controls. 130*s.* (post 3*s.* 6*d.*)
Vol. III. Flutter and Vibration, Instruments, Miscellaneous, Parachutes, Plates and Panels, Propulsion. 130*s.* (post 3*s.* 3*d.*)
Vol. IV. Stability, Structures, Wind Tunnels, Wind Tunnel Technique. 130*s.* (post 3*s.* 3*d.*)

1946 Vol. I. Accidents, Aerodynamics, Aerofoils and Hydrofoils. 168*s.* (post 3*s.* 9*d.*)
Vol. II. Airscrews, Cabin Cooling, Chemical Hazards, Controls, Flames, Flutter, Helicopters, Instruments and Instrumentation, Interference, Jets, Miscellaneous, Parachutes. 168*s.* (post 3*s.* 3*d.*)
Vol. III. Performance, Propulsion, Seaplanes, Stability, Structures, Wind Tunnels. 168*s.* (post 3*s.* 6*d.*)

1947 Vol. I. Aerodynamics, Aerofoils, Aircraft. 168*s.* (post 3*s.* 9*d.*)
Vol. II. Airscrews and Rotors, Controls, Flutter, Materials, Miscellaneous, Parachutes, Propulsion, Seaplanes, Stability, Structures, Take-off and Landing. 168*s.* (post 3*s.* 9*d.*)

1948 Vol. I. Aerodynamics, Aerofoils, Aircraft, Airscrews, Controls, Flutter and Vibration, Helicopters, Instruments, Propulsion, Seaplane, Stability, Structures, Wind Tunnels. 130*s.* (post 3*s.* 3*d.*)
Vol. II. Aerodynamics, Aerofoils, Aircraft, Airscrews, Controls, Flutter and Vibration, Helicopters, Instruments, Propulsion, Seaplane, Stability, Structures, Wind Tunnels. 110*s.* (post 3*s.* 3*d.*)

Special Volumes

Vol. I. Aero and Hydrodynamics, Aerofoils, Controls, Flutter, Kites, Parachutes, Performance, Propulsion, Stability. 126*s.* (post 3*s.*)
Vol. II. Aero and Hydrodynamics, Aerofoils, Airscrews, Controls, Flutter, Materials, Miscellaneous, Parachutes, Propulsion, Stability, Structures. 147*s.* (post 3*s.*)
Vol. III. Aero and Hydrodynamics, Aerofoils, Airscrews, Controls, Flutter, Kites, Miscellaneous, Parachutes, Propulsion, Seaplanes, Stability, Structures, Test Equipment. 189*s.* (post 3*s.* 9*d.*)

Reviews of the Aeronautical Research Council

1939–48 3*s.* (post 6*d.*) 1949–54 5*s.* (post 5*d.*)

Index to all Reports and Memoranda published in the Annual Technical Reports

1909–1947 R. & M. 2600 (out of print)

Indexes to the Reports and Memoranda of the Aeronautical Research Council

Between Nos. 2351–2449	R. & M. No. 2450	2*s.* (post 3*d.*)
Between Nos. 2451–2549	R. & M. No. 2550	2*s.* 6*d.* (post 3*d.*)
Between Nos. 2551–2649	R. & M. No. 2650	2*s.* 6*d.* (post 3*d.*)
Between Nos. 2651–2749	R. & M. No. 2750	2*s.* 6*d.* (post 3*d.*)
Between Nos. 2751–2849	R. & M. No. 2850	2*s.* 6*d.* (post 3*d.*)
Between Nos. 2851–2949	R. & M. No. 2950	3*s.* (post 3*d.*)
Between Nos. 2951–3049	R. & M. No. 3050	3*s.* 6*d.* (post 3*d.*)
Between Nos. 3051–3149	R. & M. No. 3150	3*s.* 6*d.* (post 3*d.*)

HER MAJESTY'S STATIONERY OFFICE

from the addresses overleaf

Printed and published by
HER MAJESTY'S STATIONERY OFFICE

To be purchased from
York House, Kingsway, London W.C.2
423 Oxford Street, London W.1
13A Castle Street, Edinburgh 2
109 St. Mary Street, Cardiff
39 King Street, Manchester 2
50 Fairfax Street, Bristol 1
35 Smallbrook, Ringway, Birmingham 5
80 Chichester Street, Belfast 1
or through any bookseller

Printed in England

S.O. Code No. 23-3310